Quantum dynamics of CO-H_2 in full dimensionality

Benhui Yang,[1] P. Zhang,[2] X. Wang,[3] P. C. Stancil,[1,*]
J. M. Bowman,[3] N. Balakrishnan,[4] and R. C. Forrey[5]

[1]*Department of Physics and Astronomy and the Center for Simulational Physics, The University of Georgia, Athens, GA 30602, USA*

[2]*Department of Chemistry, Duke University, Durham, NC 27708, USA*

[3]*Department of Chemistry, Emory University, Atlanta, GA 30322, USA*

[4]*Department of Chemistry, University of Nevada Las Vegas, Las Vegas, NV 89154, USA*

[5]*Department of Physics, Penn State University, Berks Campus, Reading, PA 19610, USA*

(Dated: February 10, 2015)

Abstract

Accurate rate coefficients for molecular vibrational transitions due to collisions with H_2, critical for interpreting infrared astronomical observations, are lacking for most molecules. Quantum calculations are the primary source of such data, but reliable values that consider all internal degrees of freedom of the collision complex have only been reported for H_2-H_2 due to the difficulty of the computations. Here we present essentially exact full-dimensional dynamics computations for rovibrational quenching of CO due to H_2 impact. Using a high-level six-dimensional potential surface, time-independent scattering calculations, within a full angular-momentum-coupling formulation, were performed for the deexcitation of vibrationally excited CO. Agreement with experimentally-determined results confirms the accuracy of the potential and scattering computations, representing the largest of such calculations performed to date. This investigation advances computational quantum dynamics studies representing initial steps toward obtaining CO-H_2 rovibrational quenching data needed for astrophysical modeling.

* stancil@physast.uga.edu

Quantum mechanical studies of inelastic processes in molecular collisions began with the development of the nearly-exact, close-coupling (CC) method for rotational transitions in atom-diatom collisions by Arthurs and Dalgarno [1] and Takayanagi [2] in the 1960s. Over the past five decades tremendous advances in computational processing power and numerical algorithms have allowed high-level computations of inelastic processes [3, 4] as well as reactive collisional dynamics of large molecular systems, the latter using primarily time-dependent approaches [5–7]. Until recently, however, the largest full-dimensional inelastic studies for a system of two colliding molecules have been limited to H_2-H_2 collisions in six-dimensions (6D), which were performed with both time-independent [8] and time-dependent [9, 10] approaches for solving the Schrödinger equation. However, to make these computations possible, the authors resorted to various angular-momentum decoupling approximations with uncertain reliability. It was only recently [11–13] that these decoupling approximations were relaxed and essentially exact full-dimensional CC computations for the H_2-H_2 system became feasible. Despite the large internal energy spacing of H_2, which allows the basis sets to be relatively compact, these calculations are computationally demanding. Replacing one H_2 molecule with a molecule that has smaller internal energy spacing, such as carbon monoxide, would further increase the computational demands. Whether the CC method could in practice be used to describe such a diatom-diatom system in full-dimensionality remains an open question.

First detected in the interstellar medium in 1970 [14], carbon monoxide is the second most abundant molecule, after H_2, in most astrophysical environments. CO has been the focus of countless theoretical astrophysical studies and observations, being detected in objects as distant as high redshift quasars [15] to cometary comae in our solar system [16] to the atmospheres of extrasolar giant planets [17]. Most studies have focused on pure rotational transitions observed in the far infrared to the radio or electronic absorption in the near ultraviolet. Over the past decade, however, near infrared (NIR) emission of CO due to the fundamental vibrational band near 4.7 μm has been detected in a variety of sources including star-forming regions in Orion with the *Infrared Space Observatory* [18] and protoplanetary disks of young stellar objects [19–21] with the Gemini Observatory and the Very Large Telescope. In addition, pure rotational transitions, but in the first two vibrationally excited states ($v_1 = 1$ and 2), were detected by the Submillimeter Array in the circumstellar shell of the much-studied evolved star IRC+10216 [22]. In particular, high resolution observations

of the CO fundamental band probe the physical conditions in the inner disk region, ∼10-20 astronomical units (AU), the site of planet formation. Detailed modeling of such environments requires state-to-state inelastic rovibrational excitation rate coefficients for CO due to H_2 collisions, but current simulations are limited to approximate scaling methods due to the dearth of explicit data [18, 23].

In this Article, we address the two issues outlined above by advancing the state-of-the-art for inelastic quantum dynamics with a full-dimensional investigation using an accurate potential energy surface relevant to this scattering process, with a particular emphasis on the important region of the van der Waals complex. This was made possible through the accurate computation and precise fitting of a 6D CO-H_2 potential energy surface (PES) in the relevant region of the formaldehyde tetra-atomic system and the further development of the inelastic diatom-diatom time-independent scattering code, TwoBC [24], which performs full angular-momentum coupling, the CC formalism [1], including vibrational degrees-of-freedom. We first briefly describe the new CO-H_2 PES and its testing through comparison of rotational excitation calculations using the 6D PES and 4D PESs (neglecting vibrational motion) and available experimental results. The full-dimensional (6D), essentially exact, computations for rovibrational quenching of CO($v_1 = 1$) due to H_2 collisions are presented resolving a two-orders-of-magnitude discrepancy between earlier 4D calculations which adopted various approximations [25–28]. Finally, the current results are consistent with the rovibrational quenching measurements for the CO-H_2 system, performed at the Oxford Physical Chemistry Laboratory from 1976-1993, which no prior calculation has yet been able to adequately explain [29–31].

RESULTS

The CO-H_2 potential energy surface. The CO-H_2 interaction has been of considerable interest to the chemical physics community for many decades with one of the first 4D surfaces for the electronic ground state constructed by Schinke *et al.* [32], which was later extended by Bačić *et al.* [25]. The group of Jankowski, Szalewicz, and coworkers performed accurate 5D and 6D electronic energy calculations, but averaged over monomer vibrational modes, and performed several fits to obtain a series of 4D rigid-rotor surfaces, referred to as the V98 [33], V04 [34], and V12 [35] PESs. A 6D PES for formaldehyde was constructed

earlier by Zhang *et al.* [36], but it was developed for reactive scattering applications and consequently, limited attention was given to the long-range CO-H_2 van der Waals configuration. Therefore as a prerequisite to 6D inelastic dynamics studies, we carried out an unprecedented potential energy calculation including over 459,756 energy points (see Methods for details). The potential energy data were then fit using the invariant polynomial method with Morse-type variables in terms of bond-distances [37, 38]. The resulting 6D PES, referred to as V6D, is shown in Fig. 1 for one sample configuration. Some features of V6D are also illustrated in Supplementary Figs. S2 - S4.

Cross sections and rate coefficients. Time-independent quantum scattering calculations were performed using the CC formulation of Arthurs and Dalgarno [1] as implemented for diatom-diatom collisions in the 4D rigid-rotor approximation in MOLSCAT [39] and extended to full-dimensional dynamics as described by Quéméner, Balakrishnan, and coworkers [12, 13] in TwoBC. In the first set of scattering calculations, the new 6D PES was tested for pure rotational excitation from CO($v_1 = 0, j_1 = 0, 1$), where v_1 and j_1 are the vibrational and rotational quantum numbers, respectively. The crossed molecular beam experiment of Antonova *et al.* [40], who obtained relative state-to-state rotational inelastic cross sections, is used as a benchmark. The experimental cross sections were determined at three center-of-mass kinetic energies (795, 860, and 991 cm^{-1}), but with an initial state distribution of CO estimated to be $75 \pm 5\%$ for $j_1 = 0$ and $25 \pm 5\%$ for $j_1 = 1$. Antonova *et al.* normalized the relative cross sections to rigid-rotor calculations done with MOLSCAT using the V04 PES of Jankowski and Szalewicz [33]. Comparison of the experiment with new 4D rigid-rotor calculations on V12 and full-dimensional calculations on V6D are shown in Fig. 2. We find no difference in the excitation cross sections when using V04 or V12, while the RMS cross section errors between the normalized experiment and the V12 and V6D calculations range from 0.56-0.89$\times 10^{-16}$ cm^2 and 0.55-0.95$\times 10^{-16}$ cm^2, respectively (See Supplementary Table S1 and Supplementary Note 1). Clearly, a 4D rigid-rotor treatment of the dynamics is sufficient for describing rotational excitation at these relatively high energies.

The importance of full dimensionality for rotational excitation becomes more evident as the collision energy is reduced (see also Supplementary Figs. S5 and S6). Low-energy excitation cross sections for the process

$$\mathrm{CO}(v_1 = 0, j_1 = 0) + \mathrm{H_2}(v_2 = 0, j_2 = 0) \rightarrow \mathrm{CO}(v_1' = 0, j_1' = 1) + \mathrm{H_2}(v_2' = 0, j_2' = 0), \quad (1)$$

or (0000)→(0100), using the notation defined in Methods, were measured by Chefdeville *et al.* [41] in a crossed-beam experiment. They obtained the excitation cross section for center of mass kinetic energies from 3.3 to 22.5 cm^{-1}. Though their energy resolution was limited, three broad features were detected near 6, 13, and 16 cm^{-1} attributed to orbiting resonances. Computed cross sections for process (1) using the 4D V12 PES and the full-dimensional V6D PES are presented in Fig. 3a. While both computations reveal numerous resonances, the resonances are generally shifted by 2-3 cm^{-1} between calculations. The energy and magnitude of the resonances are very sensitive to the details of the PESs, but differences may also be due to the relaxation of the rigid-rotor approximation with the use of V6D in TwoBC. In Fig. 3b, the two calculations are convolved over the experimental energy resolution and compared to the measured relative cross sections. Except for the peak near 8 cm^{-1}, the current 6D calculation appears to reproduce the main features of the experiment. RMS errors are found to be 0.355 and 0.228×10^{-16} cm^2 for the V12 and V6D PESs, respectively. Further details on the rotational excitation calculations can be found in Supplementary Note 1.

Now that the improved performance of the V6D potential for pure rotational excitation is apparent, we turn to rovibrational transitions. As far as we are aware, prior experimental [29–31, 42, 43] and theoretical [25–28] studies are limited to the total quenching of CO($v_1 = 1$). In the scattering calculations of both Bačić *et al.* [25, 26] and Reid *et al.* [27], the 4D potential of Bačić *et al.* [25] was adopted, in which two coordinates were fixed ($r_2 = 1.4$ a_0, $\phi = 0$), and various combinations of angular-momentum decoupling approximations for the dynamics were utilized (e.g., the infinite order sudden, IOS, and coupled-states, CS, approximations; see Supplementary Note 2). More recently, Flower [28] performed CC calculations on a parameterization of the 4D PES of Kobaysashi *et al.* [44]. These four sets of 4D calculations for quenching due to para-H_2 ($j_2 = 0$) are compared in Fig. 4 to the current 6D/CC calculations on the V6D surface for the case of $j_2 = j_2' = 0$. Corresponding state-to-state and total cross sections for collisions with ortho-H_2 are given in Supplementary Figs. S7-S9 with further details in Supplementary Note 2

A cursory glance at Fig. 4 reveals a more than two orders of magnitude discrepancy among the various calculations. The large dispersion for the previous calculations is due to a combination of reduced dimensionality and decoupled angular momentum which makes it difficult to assess the reliability of each approximation. The current results, however, remove

these uncertainties by utilizing i) a full-dimensional (6D) PES, ii) full-dimensional (6D) dynamics, and iii) full angular-momentum coupling. The sharp peaks in the cross sections over the 1-10 cm^{-1} range in the 6D/CC results are due to resonances [45, 46] supported by the CO-H_2 van der Waals potential well. These resonances, in the rovibrational quenching of CO by H_2, are reported here for the first time and their prediction is made possible through our high-level treatment of the dynamics. Computations for transitions involving other initially excited j_2 states and inelastic H_2 ($j_2 \neq j_2'$) transitions are presented and compared in Supplementary Figs. S10 and S11 and Supplementary Note 2.

Using the current 6D/CC cross sections and the 4D/IOS-CS results of Reid *et al.*, rate coefficients for a Maxwellian velocity distribution are computed and compared in Fig. 5 to total deexcitation measurements [29–31] reported by Reid *et al.* [27]. The comparison is not straight-forward because i) the measurements correspond to an initial thermal population of H_2 rotational states, ii) the initial rotational population of CO($v_1 = 1, j_1$) was unknown, iii) the experimental rate coefficients for ortho-H_2 are estimated from para- and normal-H_2 measurements, and iv) the contribution from a quasi-resonant channel,

$$\mathrm{CO}(v_1 = 1) + \mathrm{H_2}(v_2 = 0, j_2 = 2) \rightarrow \mathrm{CO}(v_1' = 0) + \mathrm{H_2}(v_2' = 0, j_2' = 6) + \Delta E, \qquad (2)$$

dominates the para-H_2 case for $T \gtrsim 50$ K. Fig. 5a displays the CO($v_1 = 1$) rovibrational deexcitation rate coefficients from the current 6D/CC calculations for collisions of ortho-H_2 for j_2=1 and 3, separately. These rate coefficients are summed over all j_1' and j_2'=1, 3, and 5. Assuming a Boltzmann average at the kinetic temperature T of the H_2 rotational levels $j_2 = 1$ and 3, presumed to be representative of the experimental conditions, rate coefficients are computed and found to be in good agreement with the measurements above 200 K. From Fig. 5a, the contribution from j_2=3 is seen to be only important above 150 K. The remaining difference with experiment at low temperatures may be due to the fact mentioned above that the ortho-H_2 rate coefficients are not directly measured, but deduced from normal-H_2 and para-H_2 experiments. In particular, Reid *et al.* assume that the ortho/para ratio in the normal-H_2 measurements is 3:1, i.e. statistical, and independent of temperature. Further, as stated above, the experimental CO rotational population distribution in $v_1 = 1$ is unknown. Nevertheless, the current 6D/CC computations are a significant advance over the 4D results of Reid *et al.* which also correspond to a Boltzmann average of rate coefficients for j_2=1 and 3.

As indicated above, the situation for para-H_2 collisions is more complicated due to the quasi-resonant contribution (2), a mechanism not important for ortho-H_2. Boltzmann-averaged rate coefficients are presented in Fig. 5b including j_2=0 and 2 summed over j_2'= 0, 2, and 4, with and without the quasi-resonant contribution, $j_2 = 2 \rightarrow j_2' = 6$. While the current 6D/CC results and the 4D calculations of Reid *et al.* are in agreement that the quasi-resonant contribution becomes important for $T \gtrsim 50$ K, the relative magnitude compared to the non-resonant transitions from the 6D/CC calculation is somewhat less than obtained previously with the 4D potential. This is partly related to the fact that the 6D/CC rate coefficients for j_2=0 are significantly larger than those of Reid *et al.* (see also the corresponding cross sections in Fig. 4 and in the Supplementary Fig. S9). Compared to the experiment, we obtain excellent agreement for $T \lesssim 150$ K, but are somewhat smaller at higher temperatures. This small discrepancy may be related to the unknown CO($v_1 = 1, j_1$) rotational population in the measurement. Nevertheless, it is only the 6D/CC computations, i.e., dynamics in full dimensionality with full angular momentum coupling, which can reproduce the measurements for both ortho- and para-H_2. Further, the computations for the quasi-resonant process (2) were the most challenging reported here due to the requirement of a very large basis set (see Supplementary Table S2) which resulted in long computation times, a large number of channels, and usage of significant disk space ($\sim$0.5 TB per partial wave). In total, the cross sections given here consumed >40,000 CPU hours.

DISCUSSION

The current investigation of the CO-H_2 inelastic collision system has been performed with the intent of minimal approximation through the computation of a high-level potential energy surface, robust surface fitting, and full-dimensional inelastic dynamics with full angular-momentum coupling. That is, within this paradigm for studying inelastic dynamics, we have advanced the state-of-the-art for diatom-diatom collisions through this unprecedented series of computations. The approach has been benchmarked against experiment for pure rotational and rovibrational transitions giving the most accurate results to date within the experimental uncertainties and unknowns. The accuracy and long-range behavior of the 6D potential energy surface is found to be comparable to previous, lower-dimensional surfaces. The agreement of the current computation for the CO($v_1 = 1$) rovibrational quenching

with measurement resolves a long-standing (more than two decades) discrepancy and justifies the requirement of a full-dimensional approach. This methodology can now, though with significant computational cost, be applied to a large range of initial rotational levels for $v_1 = 1$ and for higher vibrational excitation to compute detailed state-to-state cross sections unobtainable via experiment.

This advance in computational inelastic scattering is particularly timely as ground-based (e.g., the Very Large Telescope (VLT)) observations have focused on CO rovibrational emission/absorption in a variety of astrophysical objects, while related observations are in the planning stages for future space-based telescopes (e.g., NASA's *James Webb Space Telescope*). In particular, we are in an exciting era of investigation into the properties of protoplanetary disks (PPDs) around young stellar objects [47]. PPDs provide the material for newly-forming stars and fledgling planets. The CO fundamental band ($|\Delta v_1| = 1$) is a tracer of warm gas in the inner regions of PPDs and, with appropriate modeling, gives insight into disk-gas kinematics and disk evolution in that zone where planets are expected to be forming. A recent survey of 69 PPDs with the VLT [19] detected CO vibrational bands in 77% of the sources including $v_1 = 1 \rightarrow 0$, $v_1 = 2 \rightarrow 1$, $v_1 = 3 \rightarrow 2$, and even $v_1 = 4 \rightarrow 3$ in a few cases. Remarkably, rotational excitation as high as $j_1 = 32$ was observed. However, the modeling of PPDs, and other astrophysical sources with CO vibrational excitation, is hindered by the lack of rate coefficients due to H_2 collisions. We are now in an excellent position to provide full-dimensional, state-to-state CO-H_2 collisional data which will not only have a profound impact on models characterizing these intriguing environments that give birth to planets, but also aid in critiquing current theories used to describe their evolution.

METHODS

Potential energy computations. The potential energy computations were performed using the explicitly correlated coupled-cluster (CCSD(T)-F12B) method [48, 49], as implemented in MOLPRO2010.1 [50]. The cc-pcvqz-f12 orbital basis sets [51] that have been specifically optimized for use with explicitly correlated F12 methods and for core-valence correlation effects have been adopted. Density fitting approximations [49] were used in all explicitly correlated calculations with the AUG-CC-PVQZ/JKFIT and AUG-CC-PWCVQZ-MP auxiliary basis sets [52, 53]. The diagonal, fixed amplitude 3C(FIX) ansatz was used,

which is orbital invariant, size consistent, and free of geminal basis set superposition error (BSSE) [54, 55]. The default CCSD-F12 correlation factor was employed in all calculations and all coupled cluster calculations assume a frozen core (C:1s and O:1s). The counter-poise (CP) correction [56] was employed to reduce BSSE. Even though the explicitly correlated calculations recover a large fraction of the correlation energy, the CP correction is still necessary, mainly to reduce the BSSE of the Hartree-Fock contribution. Benchmark calculations at the CCSD(T)-F12b/cc-pcvqz-f12 level were carried out on selected molecular configurations and results were compared with those from the conventional CCSD(T) method using aug-cc-pV5Z and aug-cc-pV6Z basis sets. Results showed that the CP corrected interaction energy agrees closely with those derived from CCSD(T)/aug-cc-pV6Z.

To construct the potential energy surface (PES), the computations were performed on a six-dimensional (6D) grid using Jacobi coordinates as shown in Supplementary Fig. S1. R is the distance between the center-of-mass of CO and H_2. r_1 and r_2 are the bond lengths of CO and H_2, respectively. θ_1 is the angle between $\mathbf{r}_1$ and $\mathbf{R}$, θ_2 the angle between $\mathbf{r}_2$ and $\mathbf{R}$, and ϕ the out-of-plane dihedral or twist angle. In the potential energy computations, the bond lengths are taken over the ranges $1.7359 \leq r_1 \leq 2.5359$ a_0 and $1.01 \leq r_2 \leq 1.81$ a_0, both with a step-size of 0.1 a_0. For R, the grid extends from 4.0 to 18.0 a_0 with step-size of 0.5 a_0 for $R < 11.0$ a_0 and 1.0 a_0 for $R > 11.0$ a_0. All angular coordinates were computed with a step-size of 15° with $0 \leq \theta_1 \leq 360°$ and $0 \leq \theta_2, \phi \leq 180°$. Additional points were added in the region of the van der Waals minimum.

The PES fit. The CO-H_2 interaction PES has been fitted in 6D using an invariant polynomial method [37, 38]. The PES was expanded in the form,

$$V(y_1 \cdots y_6) = \sum_{n1 \cdots n6}^{N} c_{n_1 \cdots n_6} y_1^{n_1} y_6^{n_6} [y_2^{n_2} y_3^{n_3} y_4^{n_4} y_5^{n_5} + y_2^{n_5} y_3^{n_4} y_4^{n_3} y_5^{n_2}], \tag{3}$$

where $y_i = e^{-0.5 d_i}$ is a Morse-type variable. The internuclear distances d_i between two atoms are defined as $d_1 = d_{HH'}$, $d_2 = d_{OH'}$, $d_3 = d_{CH'}$, $d_4 = d_{CH}$, $d_5 = d_{OH}$, and $d_6 = d_{CO}$. The total power of the polynomial, $N = n_1 + n_2 + n_3 + n_4 + n_5 + n_6$, was restricted to 6. Expansion coefficients $c_{n_1 \cdots n_6}$ were obtained using weighted least-squares fitting for potential energies up to 10,000 cm^{-1}. The root-mean-square (RMS) error in the fit of the PES is 14.22 cm^{-1}

which included 398,218 different geometries. This RMS error can be compared to that of 277 cm^{-1} for the 6D reactive surface of Zhang *et al.* [36]. From the computed energy points, the global minimum of the total potential corresponds to the collinear arrangement H-H-C-O ($\theta_1 = 0, \theta_2 = 0, \phi = 0$) with a depth of -85.937 cm^{-1} at $R = 8.0$ a_0 with r_1 and r_2 at their respectively equilibrium positions. This compares to the global minimum of the interaction potential obtained by Jankowski *et al.* [35] from their fitted V12 PES averaged over r_1 and r_2: $R = 7.911$ a_0 and -93.651 cm^{-1}. Note that this comparison is only suggestive as the global minimum in the total and interaction potentials coincide only when bond-lengths (r_1 and r_2) are fixed at their equilibrium values as illustrated in Fig. 1 and which is not the case for V12.

Scattering theory and computational details. The quantum scattering theory for a collision of an S-state atom with a rigid-rotor was developed [2, 57–59] based on the close-coupling (CC) formulation of Arthurs and Dalgarno [1]. Details about its extension to diatom-diatom collisions with full vibrational motion can be found in Refs. [12, 13]. In this approach, the interaction potential $V(R, r_1, r_2, \theta_1, \theta_2, \phi)$ is expanded as,

$$V(R, r_1, r_2, \theta_1, \theta_2, \phi) = \sum_{\lambda_1 \lambda_2 \lambda_{12}} A_{\lambda_1,\lambda_2,\lambda_{12}}(r_1, r_2, R) Y_{\lambda_1,\lambda_2,\lambda_{12}}(\hat{r}_1, \hat{r}_2, \hat{R}), \tag{4}$$

with the bi-spherical harmonic function expressed as,

$$\begin{aligned} Y_{\lambda_1,\lambda_2,\lambda_{12}}(\hat{r}_1, \hat{r}_2, \hat{R}) = & \sum_{m_{\lambda_1} m_{\lambda_2} m_{\lambda_{12}}} \langle \lambda_1 m_{\lambda_1} \lambda_2 m_{\lambda_2} | \lambda_{12} m_{\lambda_{12}} \rangle \\ & \times Y_{\lambda_1 m_{\lambda_1}}(\hat{r}_1) Y_{\lambda_2 m_{\lambda_2}}(\hat{r}_2) Y^*_{\lambda_{12} m_{\lambda_{12}}}(\hat{R}), \end{aligned} \tag{5}$$

where $0 \leq \lambda_1 \leq 10$, $0 \leq \lambda_2 \leq 6$ was used in the scattering calculations. Due to the symmetry of H_2, only even values of λ_2 contribute.

For convenience, the combined molecular state (CMS) notation is applied to describe a combination of rovibrational states for the two diatoms. A CMS represents a unique quantum state of the diatom - diatom system before or after a collision. The CMS will be denoted as $(v_1 j_1 v_2 j_2)$. v and j are the vibrational and rotational quantum numbers.

The rovibrational state-to-state cross section as a function of collision energy E is given

by,

$$\sigma_{v_1 j_1 v_2 j_2 \to v_1' j_1' v_2' j_2'}(E) = \frac{\pi}{(2j_1+1)(2j_2+1)k^2} \times \sum_{j_{12} j_{12}' l l' J \varepsilon_I} (2J+1) |\delta_{v_1 j_1 v_2 j_2 l, v_1' j_1' v_2' j_2' l'} - S^{J\varepsilon_I}_{v_1 j_1 v_2 j_2 l, v_1' j_1 v_2' j_2' l'}(E)|^2, \quad (6)$$

where $(v_1 j_1 v_2 j_2)$ and $(v_1' j_1' v_2' j_2')$ are, respectively, the initial and final CMSs of CO-H_2, the wave vector $k^2 = 2\mu E/\hbar^2$, and S is the scattering matrix. l is the orbital angular momentum and J the total collision system angular momentum, where $\mathbf{J} = \mathbf{l} + \mathbf{j}_{12}$ and $\mathbf{j}_{12} = \mathbf{j}_1 + \mathbf{j}_2$.

Thorough convergence testing was performed in the scattering calculations by varying all relevant parameters. The CC equations were propagated for each value of R from 4 to 18.0 a_0 using the log-derivative matrix propagation method of Johnson [60] and Manolopoulos [61], which was found to converge for a radial step-size of $\Delta R = 0.05$ a_0. The convergence tests of the $v_1 = 1 \to 0$ vibrational quenching cross section of CO with respect to the number of $v_1 = 1$ rotational channels found that at least 13-15 channels have to be included in the $v_1 = 1$ basis set, especially for low-energy scattering. Based on convergence tests with respect to the adopted maximum R for the long range part of the PES, we found that the cross sections are converged down to the lowest collision energy of 0.1 cm^{-1}. This value also guarantees that the rate coefficients are converged for temperatures greater than 1 K. The number of discrete variable representation points N_{r_1} and N_{r_2}; the number of points in θ_1 and θ_2 for Gauss-Legendre quadrature, N_{θ_1} and N_{θ_2}; and the number of points in ϕ for Gauss-Hermite quadrature, N_ϕ, which were applied to project out the potential expansion coefficients were all tested for convergence with the final adopted values given in Supplementary Table S2. The basis sets and the maximum number of coupled channels are also presented in Supplementary Table S2.

The resulting integral cross sections were thermally averaged over a Maxwellian kinetic energy distribution to yield state-to-state rate coefficients as function of temperature T,

$$k_{v_1 j_1 v_2 j_2 \to v_1' j_1' v_2' j_2'}(T) = \left(\frac{8}{\pi m \beta}\right)^{1/2} \beta^2 \int_0^\infty E \sigma_{v_1 j_1 v_2 j_2 \to v_1' j_1' v_2' j_2'}(E) \exp(-\beta E) dE, \quad (7)$$

where m is the reduced mass of the CO-H_2 complex, $\beta = (k_B T)^{-1}$, and k_B is Boltzmann's constant.

References

[1] Arthurs, A. M. & Dalgarno, A. The theory of scattering by a rigid rotor. *Proc. R. Soc.* **A 256**, 540-551 (1960).

[2] Takayanagi, K. The production of rotational and vibrational transitions in encounters between molecules. *Adv. At. Mol. Phys.* **1**, 149-194 (1965).

[3] Dubernet, M.-L., et al. BASECOL2012: A collisional database repository and web service within the Virtual Atomic and Molecular Data Centre (VAMDC). *Astron. Astrophys.* **553**, A50 1-14 (2013).

[4] Roueff, E. & Lique, F. Molecular excitation in the Interstellar Medium: recent advances in collisional, radiative, and chemical processes. *Chem. Rev.* **113**, 8906-8938 (2013).

[5] Althorpe, S. C. & Clary, D. C. Quantum scattering calculations on chemical reactions. *Annu. Rev. Phys. Chem.* **54**, 493-529 (2003).

[6] Bhattacharya, S., Panda, A. N., & Meyer, H.-D. Multiconfiguration time-dependent Hartree approach to study the OH + H_2 reaction. *J. Chem. Phys.* **132**, 214304 (2010).

[7] Bhattacharya, S., Kirwai, A., Panda, A. N., & Meyer, H.-D. Full dimensional quantum scattering study of the CN + H_2 reaction. *J. Chem. Sci.* **124**, 65-73 (2012).

[8] Pogrebnya, S. K. & Clary, D. C. A full-dimensional quantum dynamical study of vibrational relaxation in H_2+H_2. *Chem. Phys. Lett.* **363**, 523-528 (2002).

[9] Panda, A. N., Otto, F., Gatti, F. & Meyer, H.-D. Rovibrational energy transfer in ortho-H_2+para-H_2 collisions. *J. Chem. Phys.* **127**, 114310 (2007).

[10] Lin, S. Y. & Guo, H. Full-dimensional quantum wave packet study of collision-induced vibrational relaxation between para-H_2. *Chem. Phys.* **289**, 191-199 (2003).

[11] Quéméner G. Balakrishnan, N, & Krems, R. V. Vibrational energy transfer in ultracold molecule-molecule collisions. *Phys. Rev. A* **77**, 030704(R) (2008).

[12] Quéméner G. & Balakrishnan, N. Quantum calculations of H_2-H_2 collisions: From ultracold to thermal energies. *J. Chem. Phys.* **130**, 114303 (2009).

[13] dos Santos, S. F., Balakrishnan, N., Lepp, S., Quéméner, G., Forrey, R. C., Hinde, R. J., & Stancil, P. C. Quantum dynamics of rovibrational transitions in H_2-H_2 collisions: Internal energy and rotational angular momentum conservation effects. *J. Chem. Phys.* **134**, 214303

(2011).

[14] Wilson, R. W., Jefferts, K. B. & Penzias, A. A. Carbon monoxide in Orion nebula. *Astrophys. J.* **161**, L43-L44 (1970).

[15] Narayanan, D. *et al.*, The nature of CO emission from $z \sim 6$ quasars. *Astrophys. J. Suppl. Ser.* **174**, 13-30 (2008).

[16] Lupu, R. E., Feldman, P. D., Weaver, H. A. & Tozzi, G.-P. The fourth positive system of carbon monoxide in the Hubble Space Telescope spectra of comets. *Astrophys. J.* **670**, 1473-1484 (2007).

[17] Swain, M. R., Vasisht, G., Tinetti, G., Bouwman, J., Chen, P., Yung, Y., Deming, D. & Deroo, P. Molecular signatures in the near-infrared dayside spectrum of HD 189733b. *Astrophys. J. Lett.* **690**, L114-L117 (2009).

[18] González-Alfonso, E., Wright, C. M., Cernicharo, J., Rosenthal, D., Boonman, A. M. S. & van Dishoeck, E. F. CO and H_2O vibrational emission toward Orion Peak 1 and Peak 2. *Astron. Astrophys.* **386**, 1074-1102 (2002).

[19] Brown, J. M., Pontoppidan, K. M., van Dishoeck, E. F., Herczerg, G. J., Blake, G. A. & Smette, A. VLT-CRIRES survey of rovibrational CO emission from protoplanetary disks. *Astrophys. J.* **770**, 94 (2013).

[20] Brittain, S. D., Najita, J. R. & Carr, J. S. Tracing the inner edge of the disk around HD 100546 with rovibrational CO emission lines. *Astrophys. J.* **702**, 85-99 (2009).

[21] Bertelsen, R. P. Hein, Kamp, I., Goto, M., van der Plas, G., Thi, W.-F., Waters, L. B. F. M., van den Ancker, M. E. & Woitke, P. CO ro-vibrational lines in HD 100546: A search for disc asymmetries and the role of fluorescence. *Astron. Astrophys.* **561**, A102 (2014).

[22] Patel, N. A., Young, K. H., Brünken, S., Menten, K. M., Thaddeus, P. & Wilson, R. W. Detection of vibrationally excited CO in IRC+10216. *Astrophys. J.* **691**, L55-L58 (2009).

[23] Thi, W. F., Kamp, I., Woitke, P., van der Plas, G., Bertelsen, R. & Wiesenfeld, L. Radiation thermo-chemical models of protoplanetary discs IV. Modelling CO ro-vibrational emission from Herbig Ae discs. *Astron. Astrophys.* **551**, A49 (2013).

[24] Krems, R. V. *TwoBC - quantum scattering program*, (University of British Columbia, Vancouver, Canada, 2006).

[25] Bačić, Z., Schinke, R. & Diercksen, G. H. F. Vibrational relaxation of CO (n=1) in collisions with H_2. I. Potential energy surface and test of dynamical approximations. *J. Chem. Phys.*

82, 236-244 (1985).

[26] Bačić, Z., Schinke, R. & Diercksen, G. H. F. Vibrational relaxation of CO (n=1) in collisions with H_2. II. Influence of H_2 rotation. *J. Chem. Phys.* **82**, 245-253 (1985).

[27] Reid, J. P., Simpson, C. J. S. M. & Quiney, H. M. The vibrational deactivation of CO(v=1) by inelastic collisions with H_2 and D_2. *J. Chem. Phys.* **106**, 4931-4944 (1997).

[28] Flower, D. R. Rate coefficients for the rovibrational excitation of CO by H_2 and He. *Mon. Not. R. Astron. Soc.* **425**, 1350-1356 (2012).

[29] Andrews, A. J. & Simpson, C. J. S. M. Vibrational relaxation of CO by H_2 down to 73 K using a chemical CO laser. *Chem. Phys. Lett.* **36**, 271-274 (1975).

[30] Andrews, A. J. & Simpson, C. J. S. M. Vibrational deactivation of CO by n-H_2, by p-H_2 and by HD measured down to 77 K using laser fluorescence. *Chem. Phys. Lett.* **41**, 565-569 (1976).

[31] Wilson, G. J., Turnidge, M. L., Solodukhin, A. S. & Simpson, C. J. S. M. The measurement of rate constants for the vibrational deactivation of $^{12}C^{16}O$ by H_2, D_2 and ^4He in the gas phase down to 35 K. *Chem. Phys. Lett.* **207**, 521-525 (1993).

[32] Schinke, R., Meyer, H., Buck, U. & Diercksen, G. H. F. A new rigid-rotor H_2-CO potential-energy surface from accurate ab initio calculations and rotationally inelastic-scattering data. *J. Chem. Phys.* **80**, 5518-5530 (1984).

[33] Jankowski, P. & Szalewicz, K. Ab initio potential energy surface and infrared spectra of H_2-CO and D_2-CO van der Waals complexes. *J. Chem. Phys.* **108**, 3554-3565 (1998).

[34] Jankowski, P. & Szalewicz, K. A new ab initio interaction energy surface and high-resolution spectra of the H_2-CO van der Waals complex. *J. Chem. Phys.* **123**, 104301 (2005).

[35] Jankowski, P., Surin, L. A., Potapov, A., Schlemmer, S., McKellar, A. R. W. & Szalewicz, K. A comprehensive experimental and theoretical study of H_2-CO spectra. *J. Chem. Phys.* **138**, 084307 (2013).

[36] Zhang, X., Zou, S., Harding, L. B. & Bowman, J. M. A global ab initio potential energy surface for formaldehyde. *J. Phys. Chem. A* **108**, 8980-8986 (2004).

[37] Braams, B. J. & Bowman, J. M. Permutationally invariant potential energy surfaces in high dimensionality. *Int. Rev. Phys. Chem.* **28**, 577-606 (2009).

[38] Bowman, J. M., Czakó, G. & Fu, B. N. High-dimensional ab initio potential energy surfaces for reaction dynamics calculations. *Phys. Chem. Chem. Phys.* **13**, 8094-8111 (2011).

[39] Hutson, J. M. & Green, S. MOLSCAT computer code, Version 14,

http://www.giss.nasa.gov/tools/molscat/ (distributed by Collaborative Computational Project No. 6 of the United Kingdom Engineering and Physical Sciences Research Council, Swindon, 1994).

[40] Antonova, S., Tsakotellis, A. P., Lin, A. & McBane, G. C. State-to-state rotational excitation of CO by H_2 near 1000 cm^{-1} collision energy. *J. Chem. Phys.* **112**, 554-559 (2000).

[41] Chefdeville, S., Stoecklin, T., Bergeat, A., Hickson, K. M., Naulin, C. & Costes, M. Appearance of low energy resonances in CO-para-H_2 inelastic collisions. *Phys. Rev. Lett.* **109**, 023201 (2012).

[42] Hooker, W. J. & Millikan, R. C. Shocktube study of vibrational relaxation in carbon monoxide for the fundamental and first overtone. *J. Chem. Phys.* **38**, 214-220 (1963).

[43] Millikan, R. C. & Osburg, L. A. Vibrational relaxation of carbon monoxide by ortho- and para-hydrogen. *J. Chem. Phys.* **41**, 2196-2197 (1964).

[44] Kobayashi, R., Amos, R. D., Reid, J. P., Quiney, H. M. & Simpson, C. J. S. M. Coupled cluster ab initio potential energy surfaces for CO$\cdots$He and CO$\cdots H_2$. *Mol. Phys.* **98**, 1995-2005 (2000).

[45] Chandler, D. W. Cold and ultracold molecules: Spotlight on orbiting resonances. *J. Chem. Phys.* **132**, 110901 (2010).

[46] Casavecchia, P. & Alexander, M. H. Uncloaking the quantum nature of inelastic molecular collisions. *Science* **341**, 1076-1077 (2013).

[47] Henning, T. & Semenov, D. Chemistry in Protoplanetary Disks. *Chem. Rev.* **113**, 9016-9042 (2013).

[48] Adler, T. B., Knizia, G. & Werner, H.-J. A simple and efficient CCSD(T)-F12 approximation. *J. Chem. Phys.* **127**, 221106 (2007).

[49] Werner, H.-J., Adler, T. B. & Manby, F. R. General orbital invariant MP2-F12 theory. *J. Chem. Phys.* **126**, 164102 (2007).

[50] Werner, H.-J. et al. MOLPRO, version 2010.1. A package of ab initio programs, http://www.molpro.net (University College Cardiff Consultants, Cardiff, UK).

[51] Hill, J. G., Mazumder, S. & Peterson, K. A. Correlation consistent basis sets for molecular core-valence effects with explicitly correlated wave functions: The atoms B-Ne and Al-Ar. *J. Chem. Phys.* **132**, 054108 (2010).

[52] Hättig, C. Optimization of auxiliary basis sets for RI-MP2 and RI-CC2 calculations: Core-valence and quintuple-zeta basis sets for H to Ar and QZVPP basis sets for Li to Kr. *Phys.*

Chem. Chem. Phys. **7**, 59-66 (2005).

[53] Weigend, F. A fully direct RI-HF algorithm: Implementation, optimised auxiliary basis sets, demonstration of accuracy and efficiency. *Phys. Chem. Chem. Phys.* **4**, 4285-4291 (2002).

[54] Tew, D. P. & Klopper, W. A comparison of linear and nonlinear correlation factors for basis set limit Moller-Plesset second order binding energies and structures of He_2, Be_2, and Ne_2. *J. Chem. Phys.* **125**, 094302 (2006).

[55] Feller, D., Peterson, K. A. & Hill, J. G. Calibration study of the CCSD(T)-F12a/b methods for C_2 and small hydrocarbons. *J. Chem. Phys.* **133**, 184102 (2010).

[56] Bernardi, F. & Boys, S. F. Calculation of small molecular interactions by differences of separate total energies - some procedures with reduced errors. *Mol. Phys.* **19**, 553 (1970).

[57] Green, S. Rotational excitation in H_2-H_2 collisions - close-coupling calculations. *J. Chem. Phys.* **62**, 2271-2277 (1975).

[58] Alexander, M. H. & DePristo, A. E. Symmetry considerations in quantum treatment of collisions between two diatomic-molecules. *J. Chem. Phys.* **66**, 2166-2172 (1977).

[59] Zarur, G. & Rabitz, H. Effective potential formulation of molecule-molecule collisions with application to H_2-H_2. *J. Chem. Phys.* **60**, 2057-2078 (1974).

[60] Johnson, B. R. Multichannel log-derivative method for scattering calculations. *J. Comp. Phys.* **13**, 445-449 (1973).

[61] Manolopoulos, D. E. An improved log derivative method for inelastic-scattering. *J. Chem. Phys.* **85**, 6425-6429 (1986).

Acknowledgements

Work at UGA and Emory was supported by NASA grant NNX12AF42G from the Astronomy and Physics Research and Analysis Program, at UNLV by NSF Grant No. PHY-1205838, and at Penn State by NSF Grant No. PHY-1203228. This study was supported in part by resources and technical expertise from the UGA Georgia Advanced Computing Resource Center (GACRC), a partnership between the UGA Office of the Vice President for Research and Office of the Vice President for Information Technology. We thank Shan-Ho Tsai (GACRC), Jeff Deroshia (UGA Department of Physics and Astronomy), and Gregg Derda (GACRC) for computational assistance.

Author contributions

BHY performed the potential energy surface (PES) fitting and scattering calculations. PZ calculated the PES. XW and JMB developed the PES fitting code. NB, RCF, and PCS extended and modified the TwoBC code for CO-H_2 rovibrational scattering calculations, while NB assisted with the scattering calculations. BHY, PCS, and PZ wrote the article with contributions from all other authors.

Additional information

Supplementary information is included in the submission.

Competing financial interests

The authors declare no competing financial interests.

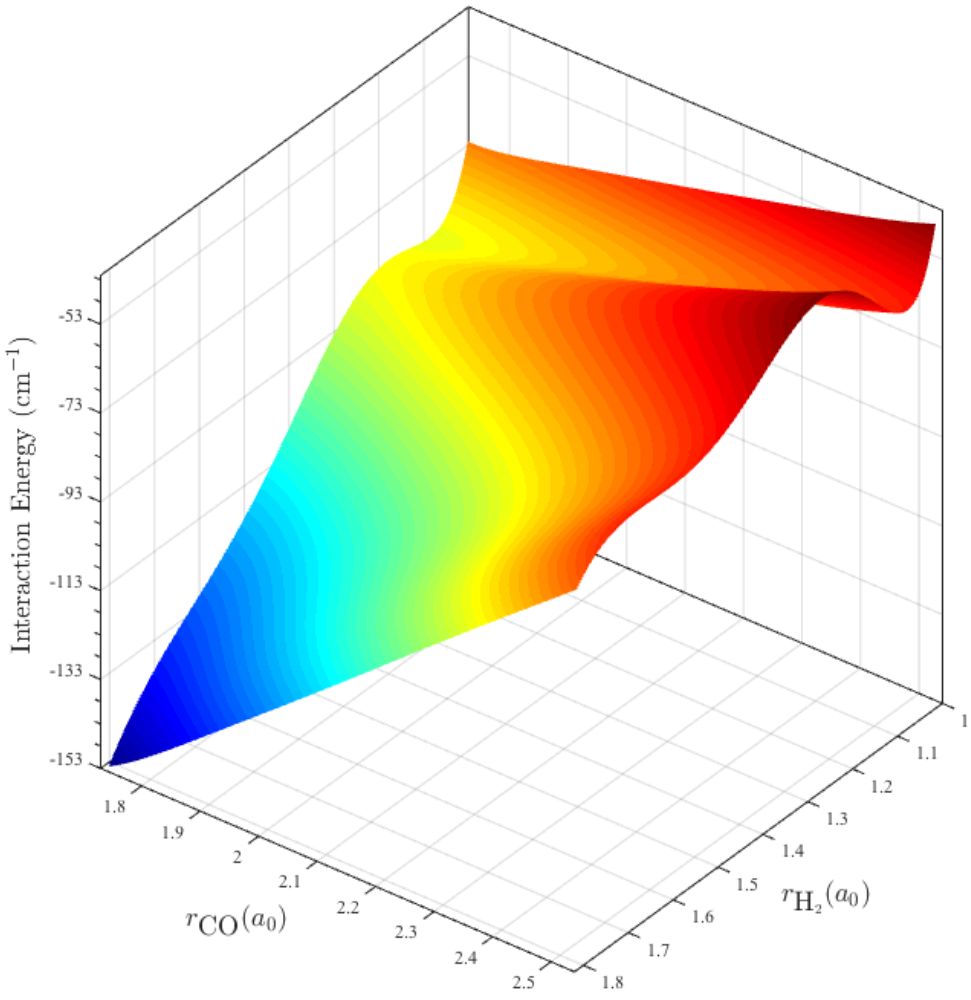

FIG. 1. **The CO-H_2 interaction potential energy surface V6D.** The potential surface is constructed in the 6D diatom-diatom Jacobi coordinates $(R, r_1, r_2, \theta_1, \theta_2, \phi)$, r_1 and r_2 are bond lengths, R the internuclear distance between CO and H_2 center of masses, θ_1 and θ_2 the angles between **R** and $\mathbf{r}_1$ and $\mathbf{r}_2$, and ϕ the dihedral or twist angle. See Supplemental Fig. 1. Here the dependence of the potential surface on bond lengths $r_{CO} = r_1$ and $r_{H_2} = r_2$ is shown with $R = 8$ a_0, $\theta_1 = 180°$, $\theta_2 = 0$, and $\phi = 0$. Note that the CO(r_1) and H_2(r_2) diatom potentials have been subtracted.

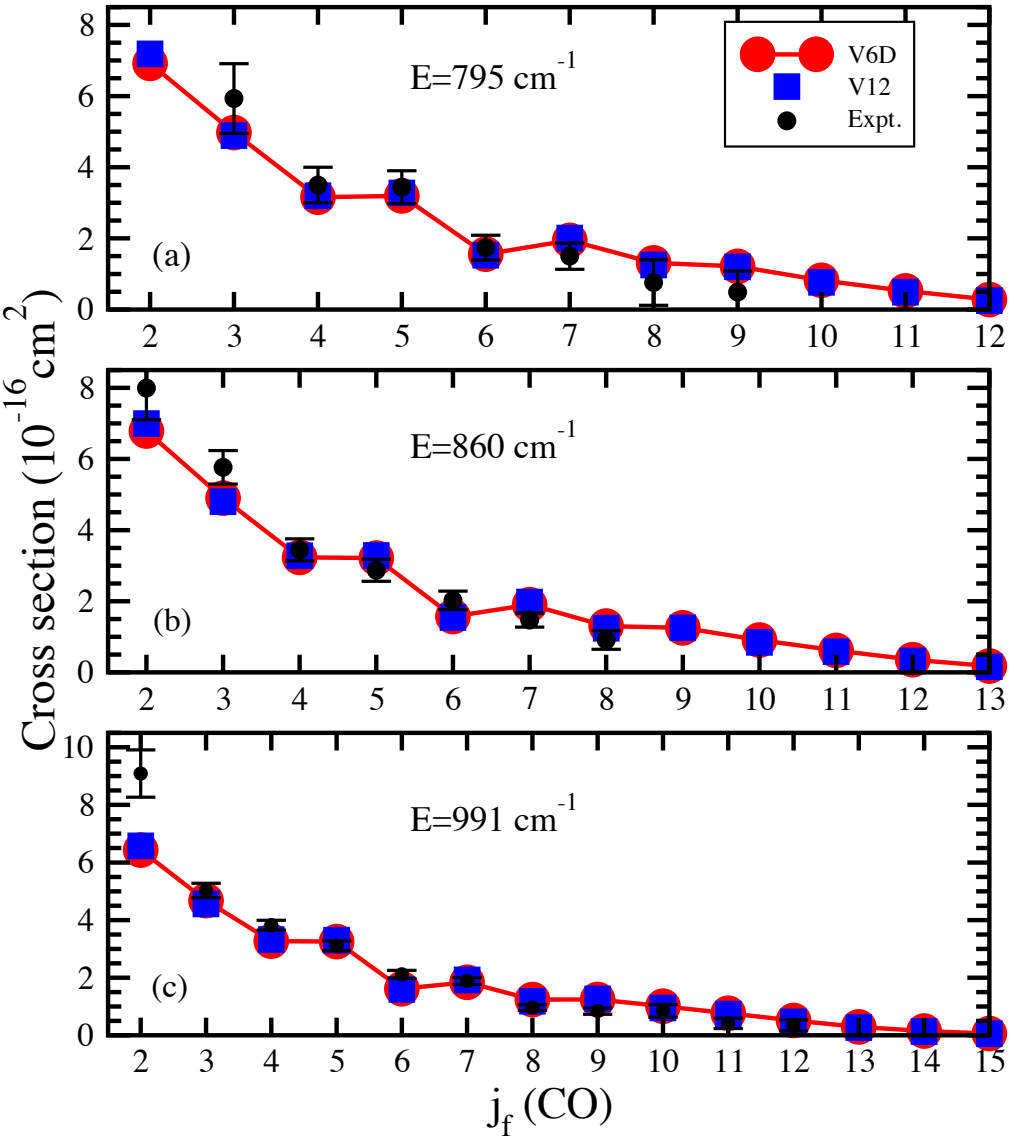

FIG. 2. **State-to-state cross sections for rotational excitation of CO($v_1 = 0, j_1 = 0, 1$) by collisions with H_2.** Theoretical results of full-dimensional calculations on V6D and 4D rigid-rotor calculations on V12 are compared with normalized experimental results [40] for collision energies of (a) 795 cm^{-1}, (b) 860 cm^{-1}, and (c) 991 cm^{-1}. The calculations were performed for $H_2(v_2 = 0, j_2 = 0)$, but the experimental H_2 rotational distribution was undetermined. The error bars correspond to twice the estimated standard deviation in the weighted means of the measurements [40].

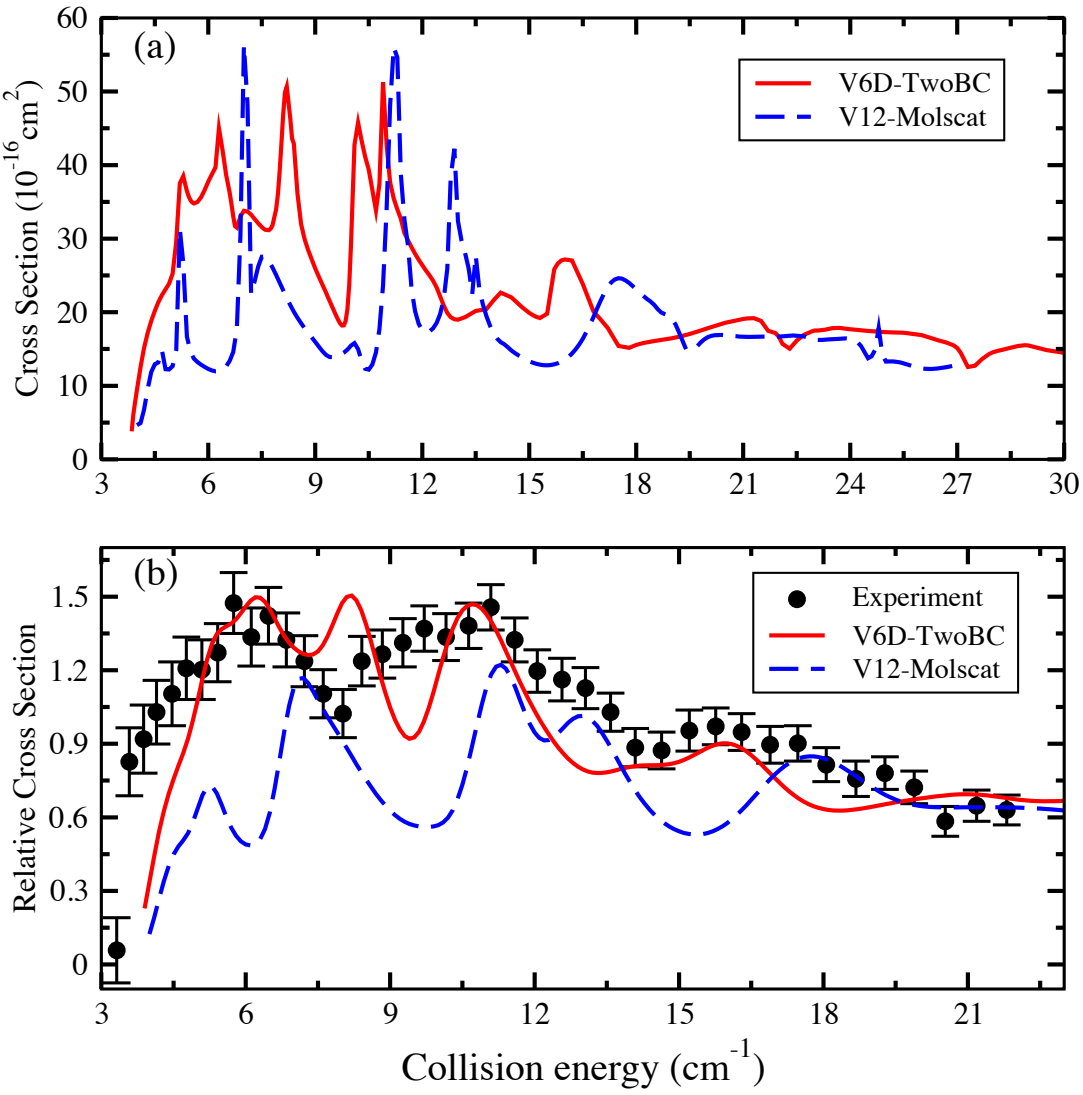

FIG. 3. **Low energy excitation cross sections.** $j_1 = 0 \rightarrow 1$ cross sections for CO($v_1 = 0$) due to collisions with $H_2(v_2 = 0, j_2 = 0)$ are shown as a function of collision energy. (a): computed cross sections using the 4D V12 and 6D V6D PESs. (b): computed cross sections convolved over the experimental beam energy spread (lines) compared to the relative experiment of Chefdeville *et al.* [41] (circles with error bars). The error bars on the experimental cross sections of Chefdeville *et al.* represent the statistical uncertainty at a 95% confidence interval.

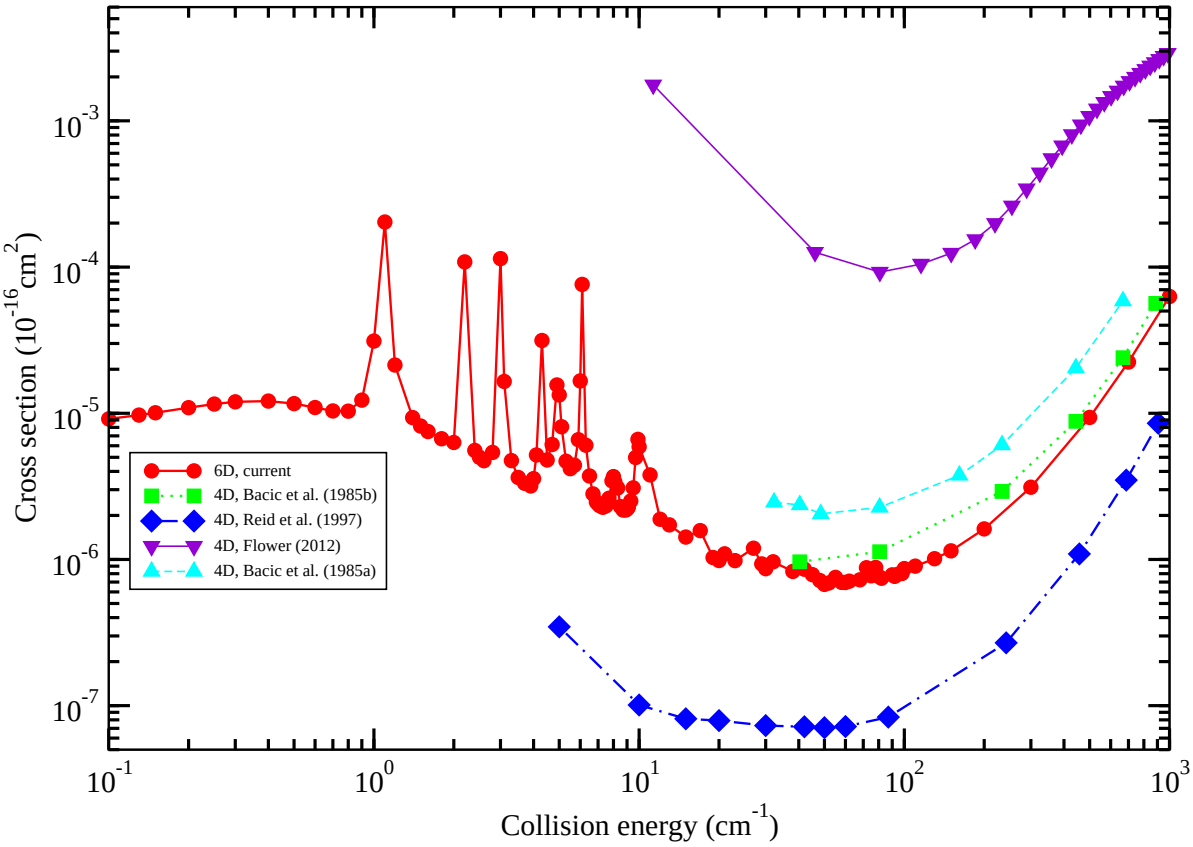

FIG. 4. **Total theoretical cross sections for the vibrational deexcitation of CO($v_1 = 1$) by para-H_2.** Current 6D/CC results are compared to previous 4D calculations. The 4D results of Bačić *et al.* [26] and Reid *et al.* [27] do not distinguish CO rotational states, while the 4D results of Bačić *et al.* [25], 4D results of Flower [28], and the current 6D/CC results are for initial $j_1 = 0$ summed over all final CO($v_1' = 0, j_1'$). In every case, the H_2 rovibrational state remains unchanged, $v_2, j_2 = v_2', j_2' = 0, 0$.

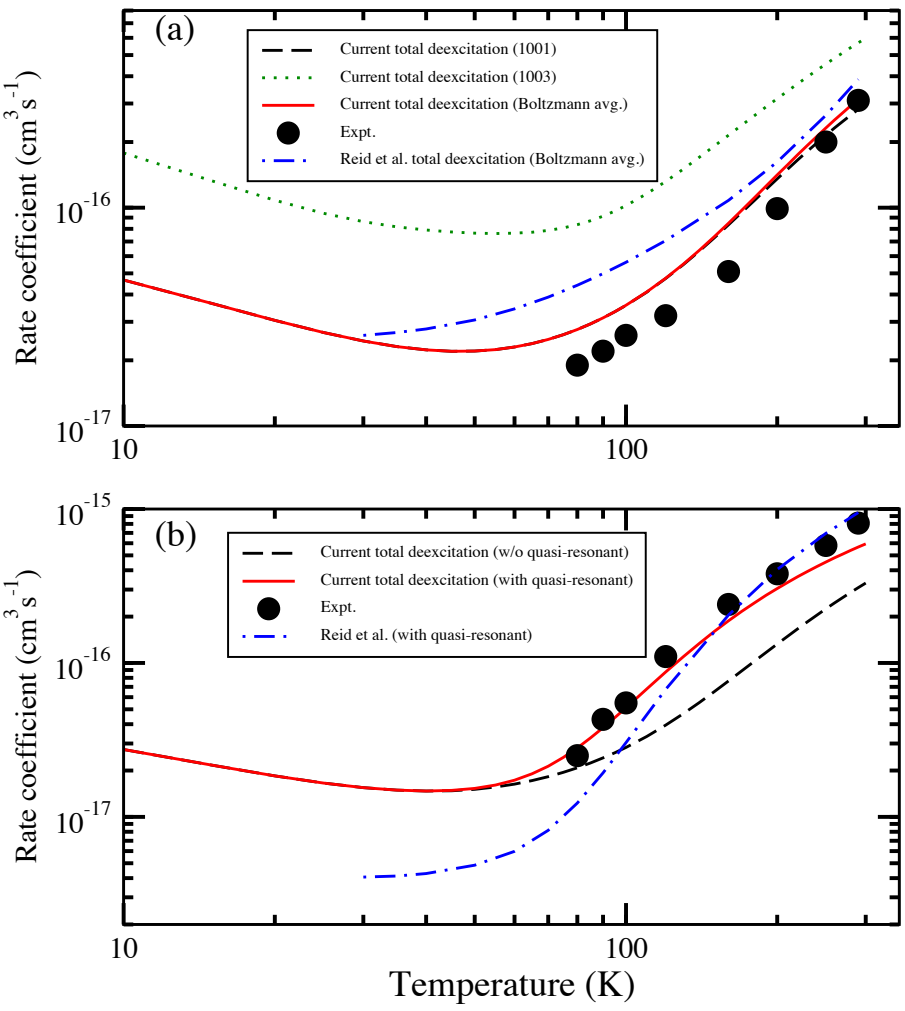

FIG. 5. **Rate coefficients for the vibrational deexcitation of CO($v_1 = 1$) due to H_2.** Current 6D/CC (solid, dashed, and dotted lines) and Reid *et al.* [27] 4D (dot-dashed line) calculations are compared to the total CO($v_1 = 1$) rovibrational quenching experiment (symbols) [29–31]. (a) Ortho-H_2 rate coefficients for initial state-resolved, $(100j_2) \rightarrow (0j_1'0j_2')$, summed over j_1' and j_2' (dashed and dotted lines) and for a Boltzmann average of initial $H_2(j_2 = 1, 3)$ (solid and dot-dashed lines). (b) Para-H_2 rate coefficients for a Boltzmann average of initial $H_2(j_2 = 0, 2)$ with and without the quasi-resonant process (2). Note that the experimental uncertainties are smaller than the symbol sizes.

Supplementary Information

SUPPLEMENTARY FIGURES

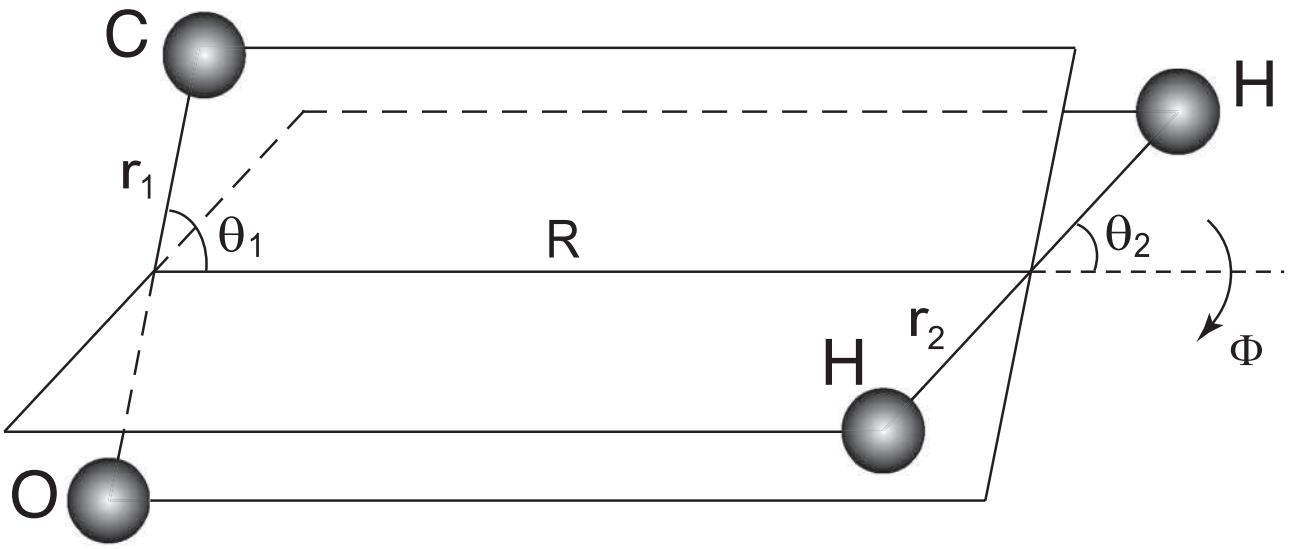

FIG. S1. The six-dimensional Jacobi coordinates for CO-H_2. r_1 and r_2 are bond lengths, R the internuclear distance between CO and H_2 center of masses, θ_1 and θ_2 the angles between $\vec{R}$ and $\vec{r_1}$ and $\vec{r_2}$, and ϕ the dihedral or twist angle.

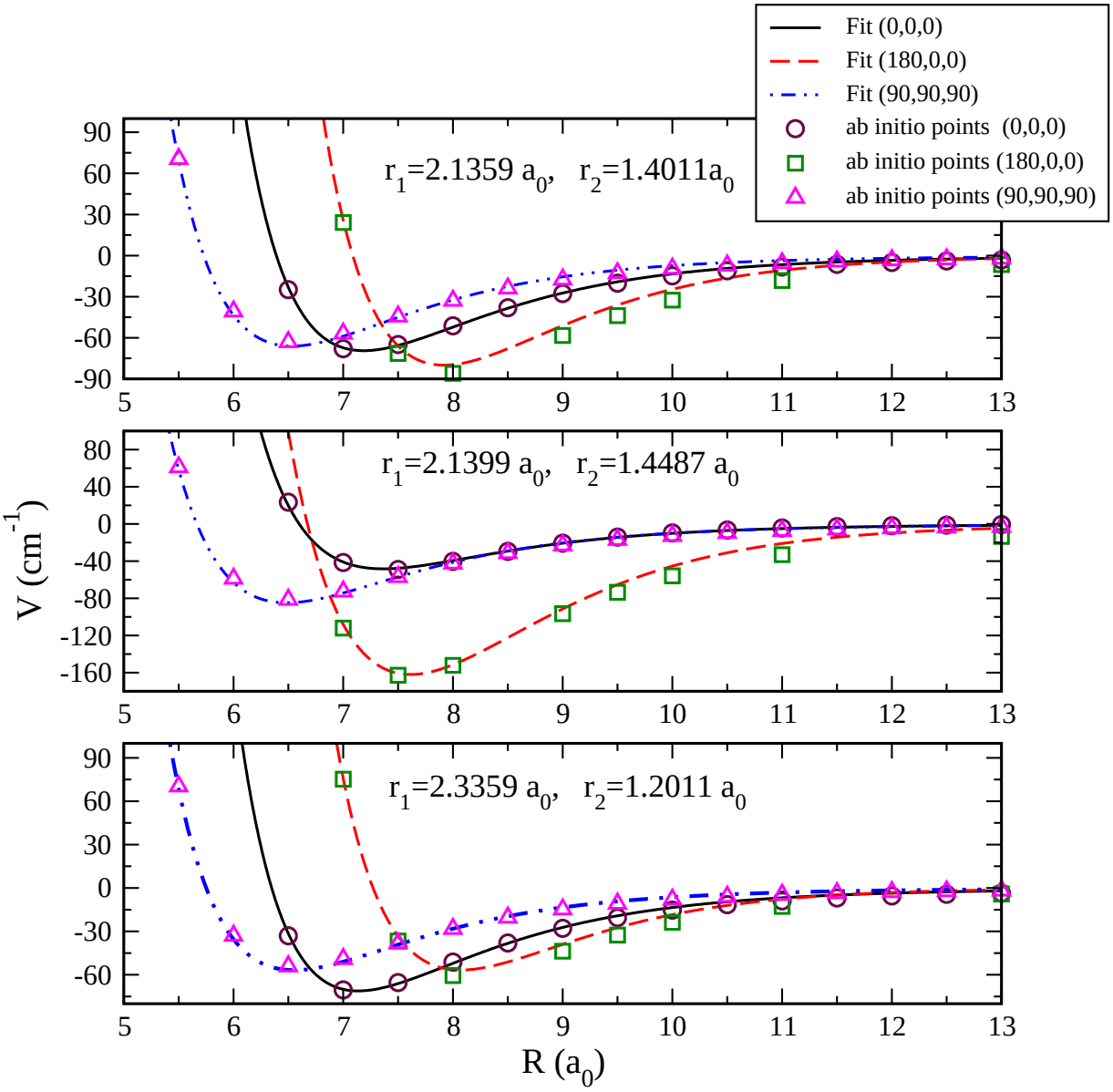

FIG. S2. Slices of the CO-H_2 interaction potential V6D. R dependence of the interaction potential V6D for representative slices with bond lengths fixed as indicated and (θ_1, θ_2, ϕ)=(0°, 0°, 0°), (180°, 0°, 0°), and (90°, 90°, 90°). V6D fit (lines), computed ab initio energy points (symbols). This figure may be compared to Fig. 2 of Ref. [S1].

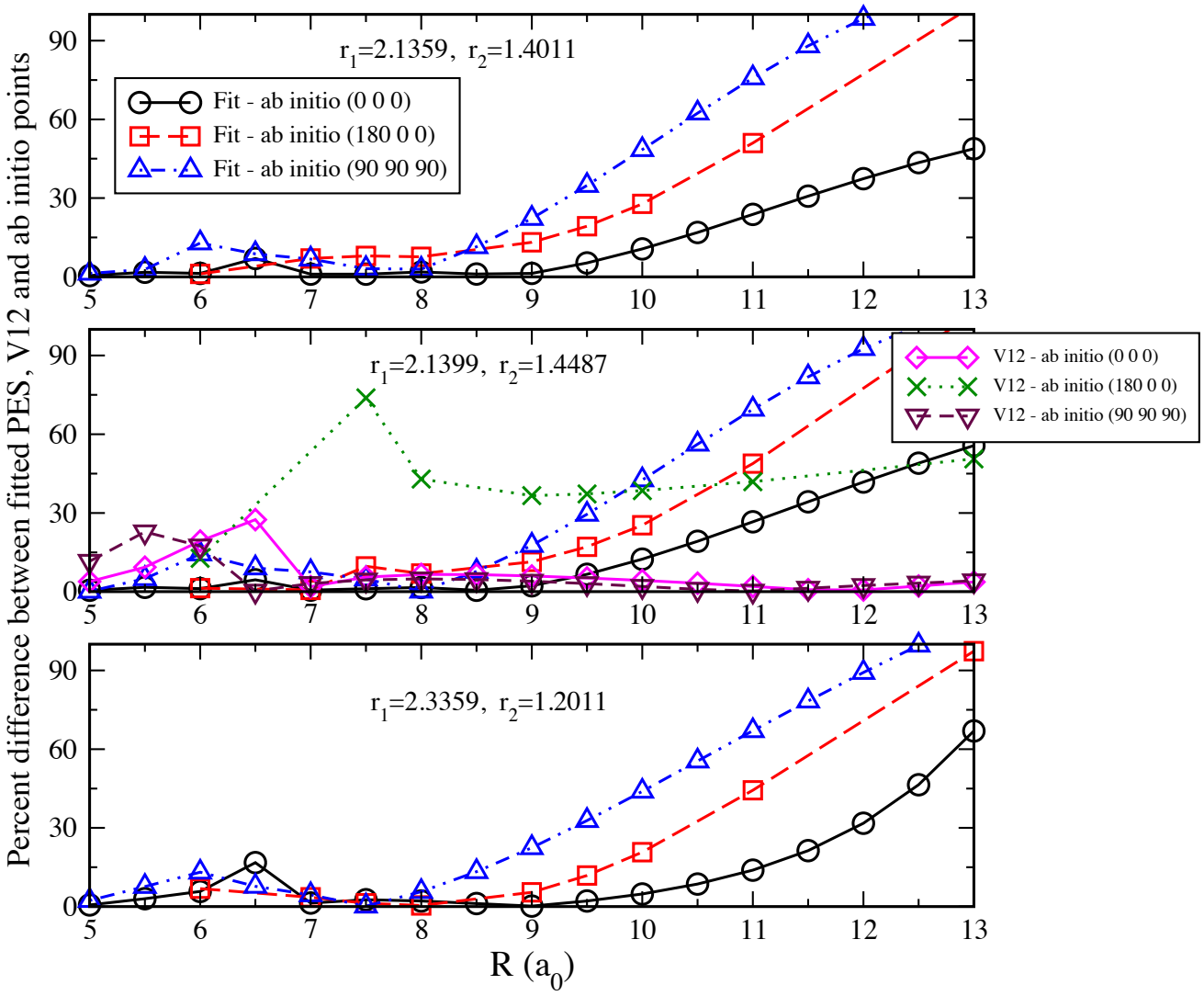

FIG. S3. Percent differences between CO-H_2 PESs. Percent difference between the fitted PES and ab initio energy points of the interaction potential V6D for representative slices with bond lengths fixed as indicated and (θ_1, θ_2, ϕ)=(0°, 0°, 0°), (180°, 0°, 0°), and (90°, 90°, 90°). The middle panel also displays the percent difference between the V12 PES and the current ab initio data. The percent differences only become large in the asymptotic limit as the PES itself approaches zero. Also, displayed in the middle panel is the difference between the V12 PES and the current ab initio data. It is seen that there is good agreement, even in the long-range limit, except for the $\theta_1 = 180°$ configuration. This difference may partly be due to the fact that V12 is a 4D PES obtained by averaging a 6D PES over the CO and H_2 ground state vibrational wave functions.

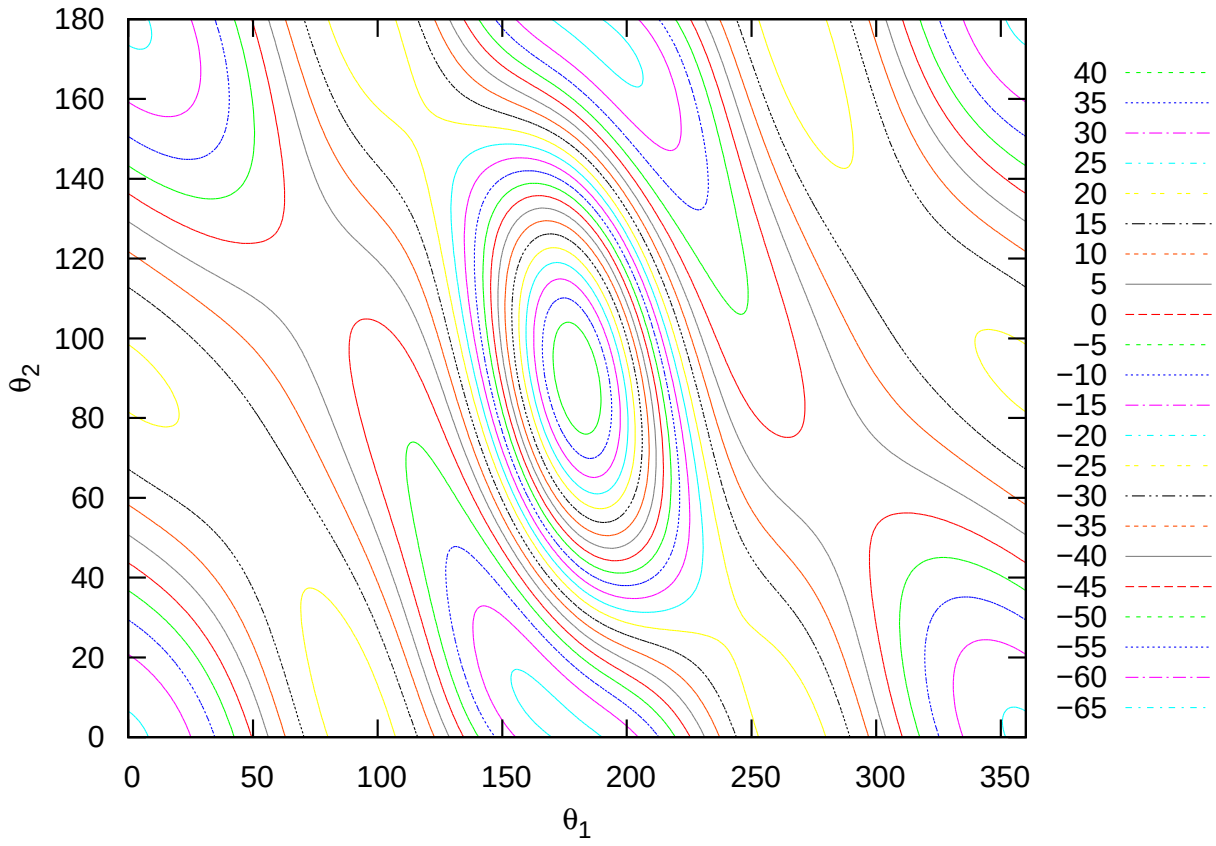

FIG. S4. Contour plot of the CO-H_2 V6D PES. The contour plot is given as a function of θ_1 and θ_2. $R = 7.5$ a_0, $\phi = 0°$, $r_1 = 2.1359$ a_0, $r_2 = 1.4011$ a_0. The legend gives the contour energies in cm^{-1}. This figure may be compared to Fig. 1 of Ref. [S1].

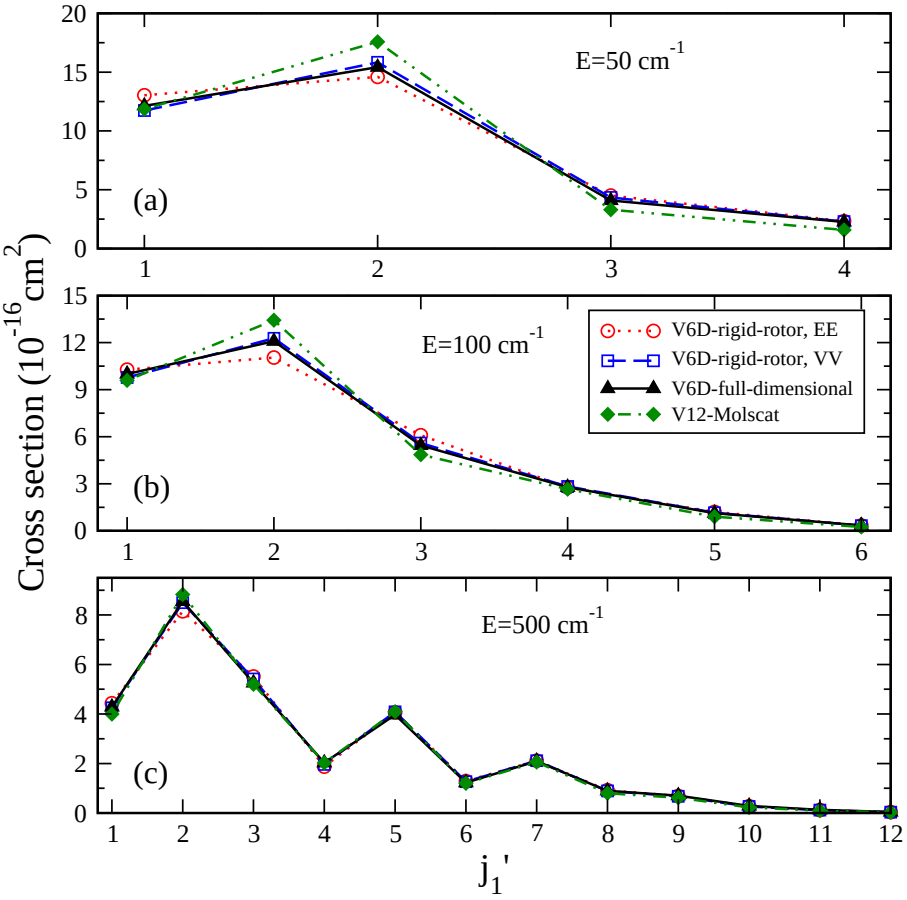

FIG. S5. CO rotational excitation cross sections due to H_2 collisions. Rigid-rotor approximation $j_1 = 0 \rightarrow j_1'$ excitation cross sections of $CO(v_1 = 0, j_1)$ by collisions with $H_2(v_2 = 0, j_2 = 0)$ using the V6D (EE and VV) and V12 potentials compared to the full-dimensional calculation. See Supplementary Note 1 for further details. Collision energy: (a) 50 cm^{-1}, (b) 100 cm^{-1}, and (c) 500 cm^{-1}.

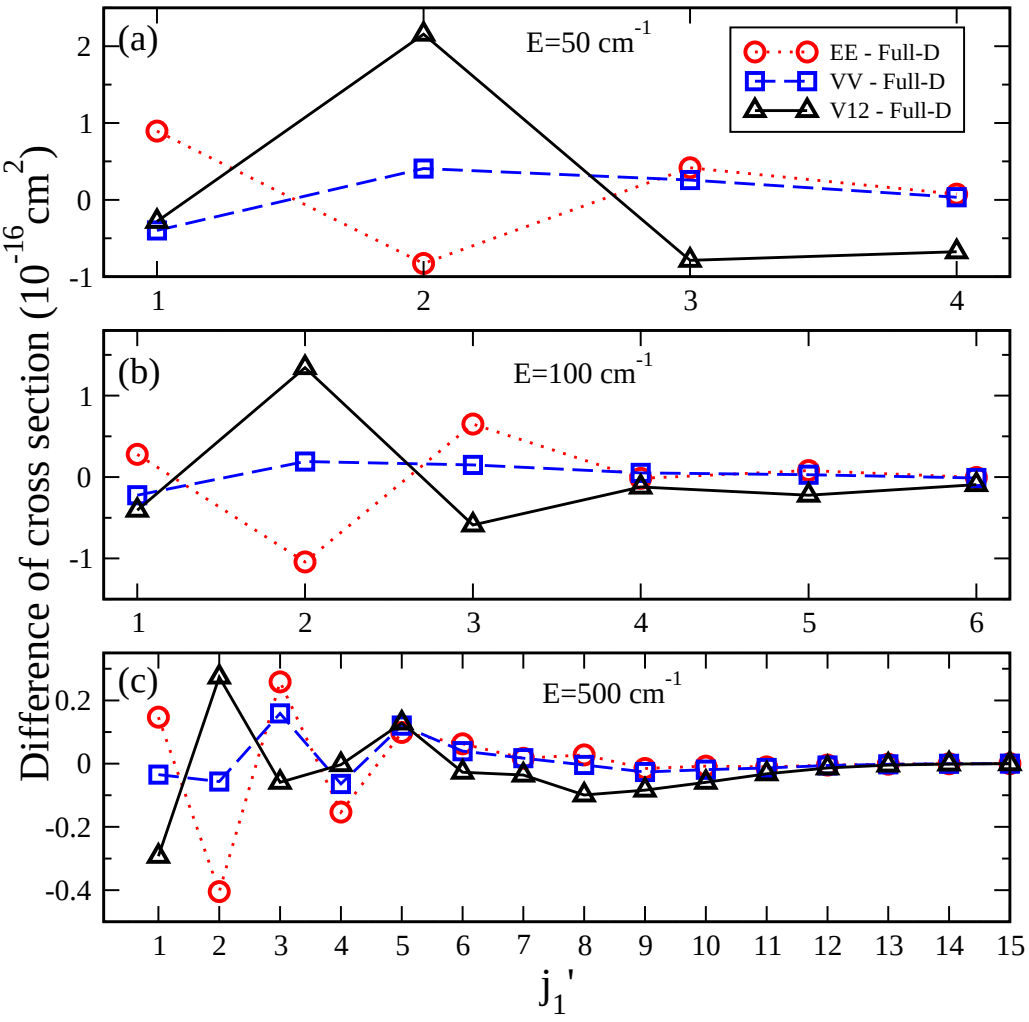

FIG. S6. CO rotational excitation cross section difference for H_2 collisions. Difference of $j_1 = 0 \rightarrow j_1'$ excitation cross sections of $CO(v_1 = 0, j_1)$ by collisions with $H_2(v_2 = 0, j_2 = 0)$ using the V6D (EE and VV), V12 potentials and those of the full-dimensional calculation (Full-D, V6D). See Supplementary Note 1 for further details. Collision energy: (a) 50 cm^{-1}, (b) 100 cm^{-1}, and (c) 500 cm^{-1}.

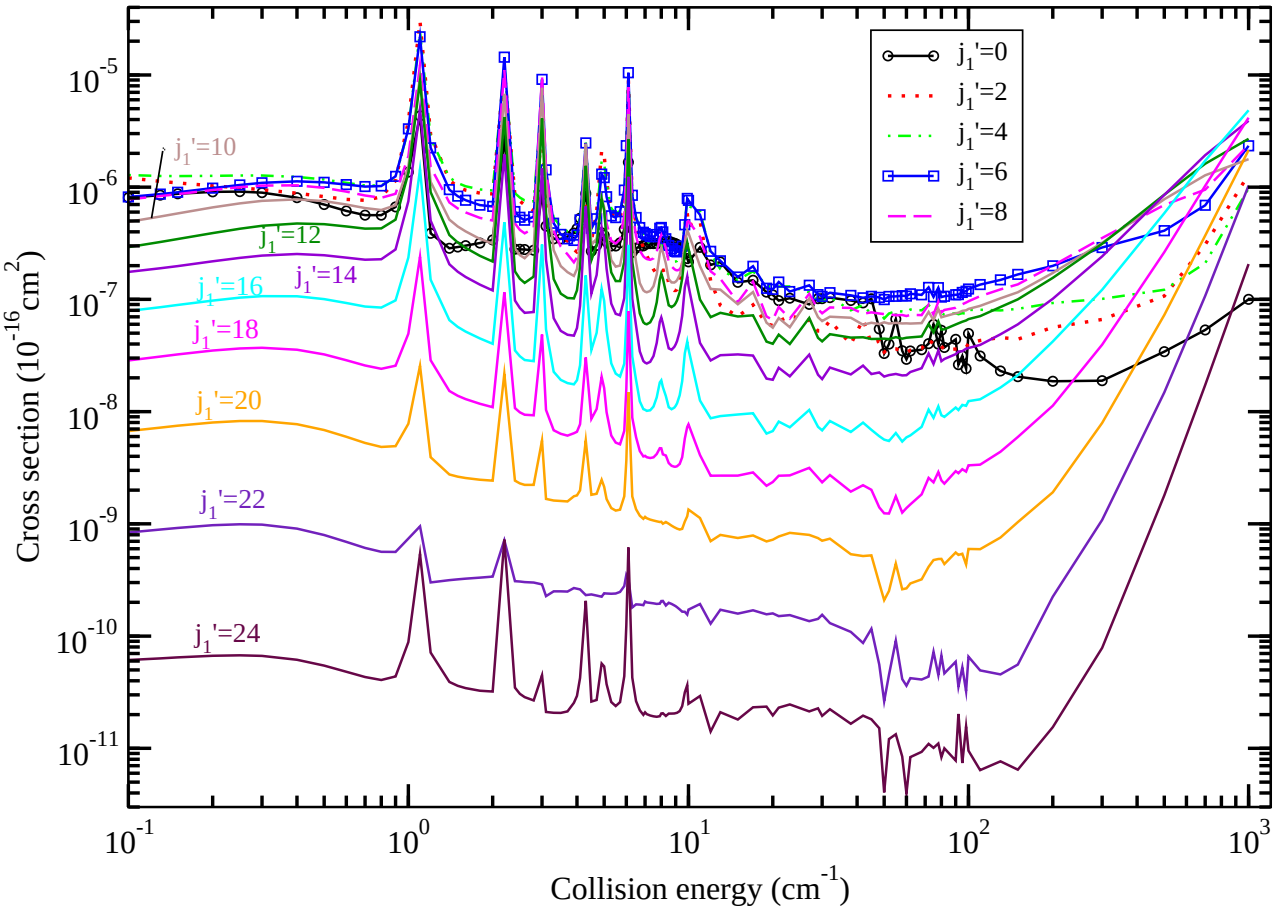

FIG. S7. CO–para-H_2 vibrational quenching state-to-state cross sections. State-to-state cross sections for the vibrational quenching of CO from $(v_1 = 1, j_1 = 0)$ to $(v_1' = 0, j_1')$, j_1'=0, 2, 4, $\cdots$, 24, due to para-$H_2(v_2 = 0, j_2 = 0)$ collisions, or in CMS notation $(1000) \rightarrow (0j_1'00)$.

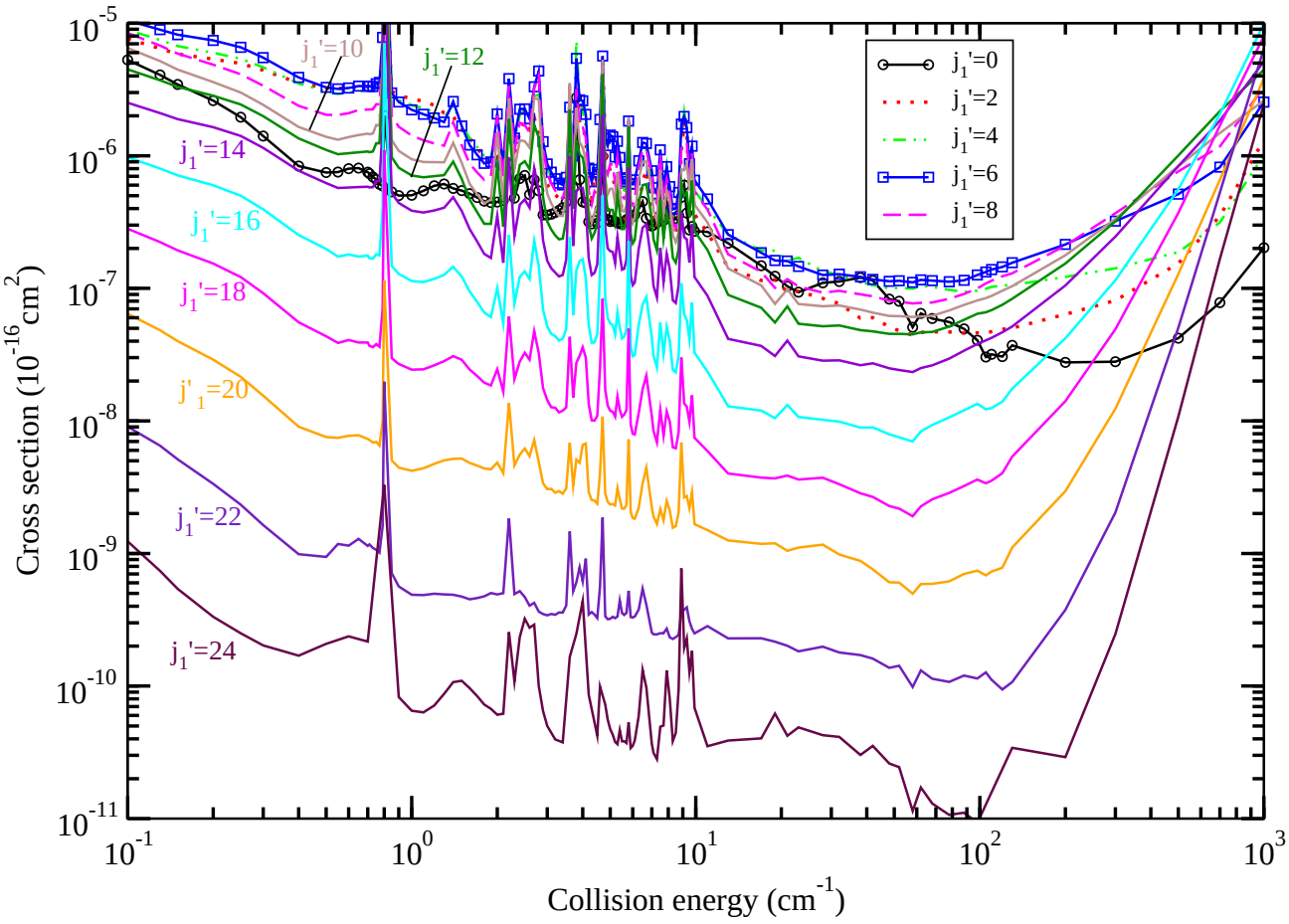

FIG. S8. CO–ortho-H_2 vibrational quenching state-to-state cross sections. State-to-state cross sections for the vibrational quenching of CO from $(v_1 = 1, j_1 = 0)$ to $(v_1' = 0, j_1')$, j_1'=0, 2, 4, $\cdots$, 24, by ortho-$H_2(v_2 = 0, j_2 = 1)$, or in CMS notation $(1001) \rightarrow (0j_1'01)$.

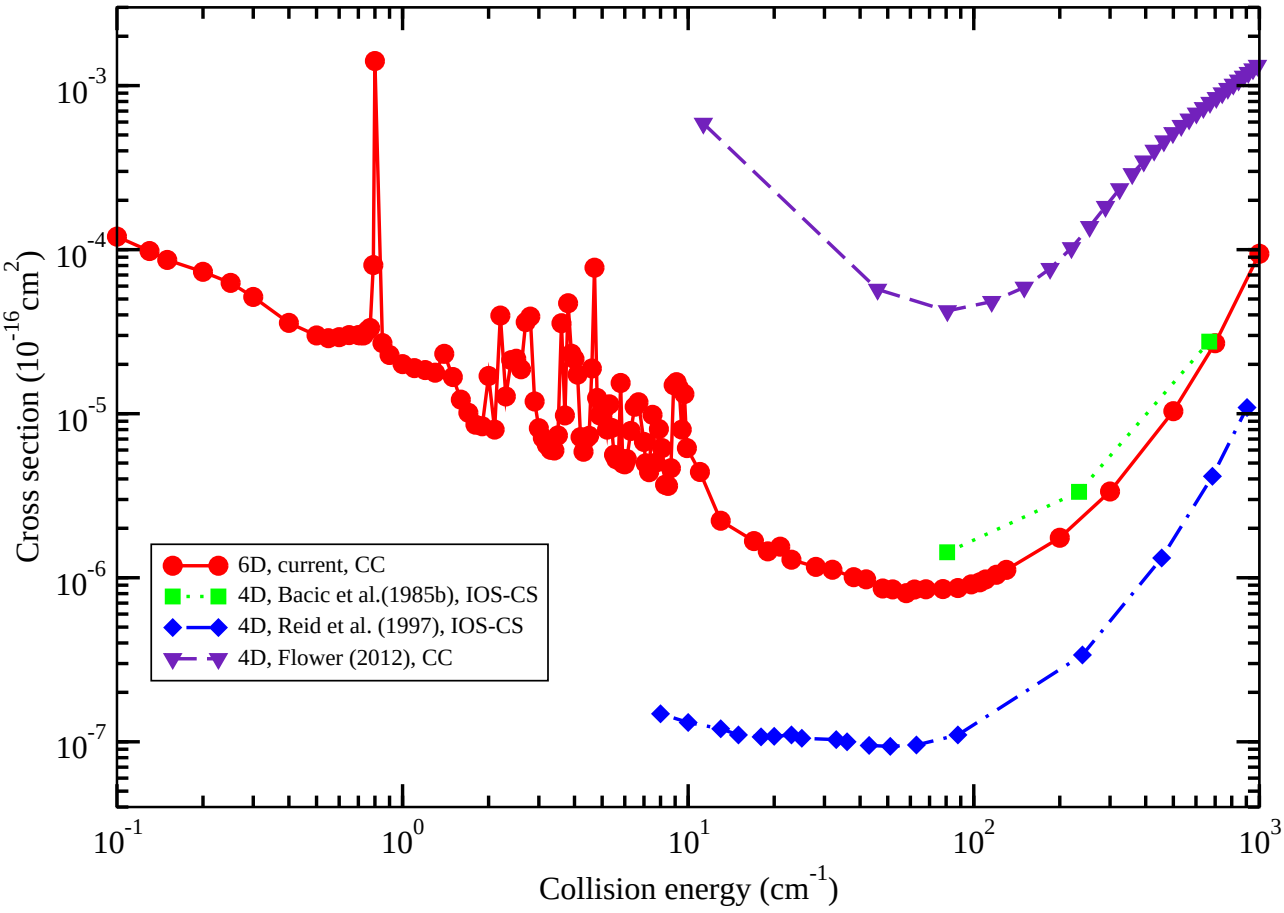

FIG. S9. Total CO–ortho-H_2 vibrational quenching cross sections. Total cross sections for the vibrational quenching of CO($v_1 = 1$) + H_2($v_2 = 0, j_2 = 1$) to CO($v_1' = 0$) + ortho-H_2($v_2' = 0, j_2'$=1). Similar to Fig. 4 of the main text, except for ortho-H_2.

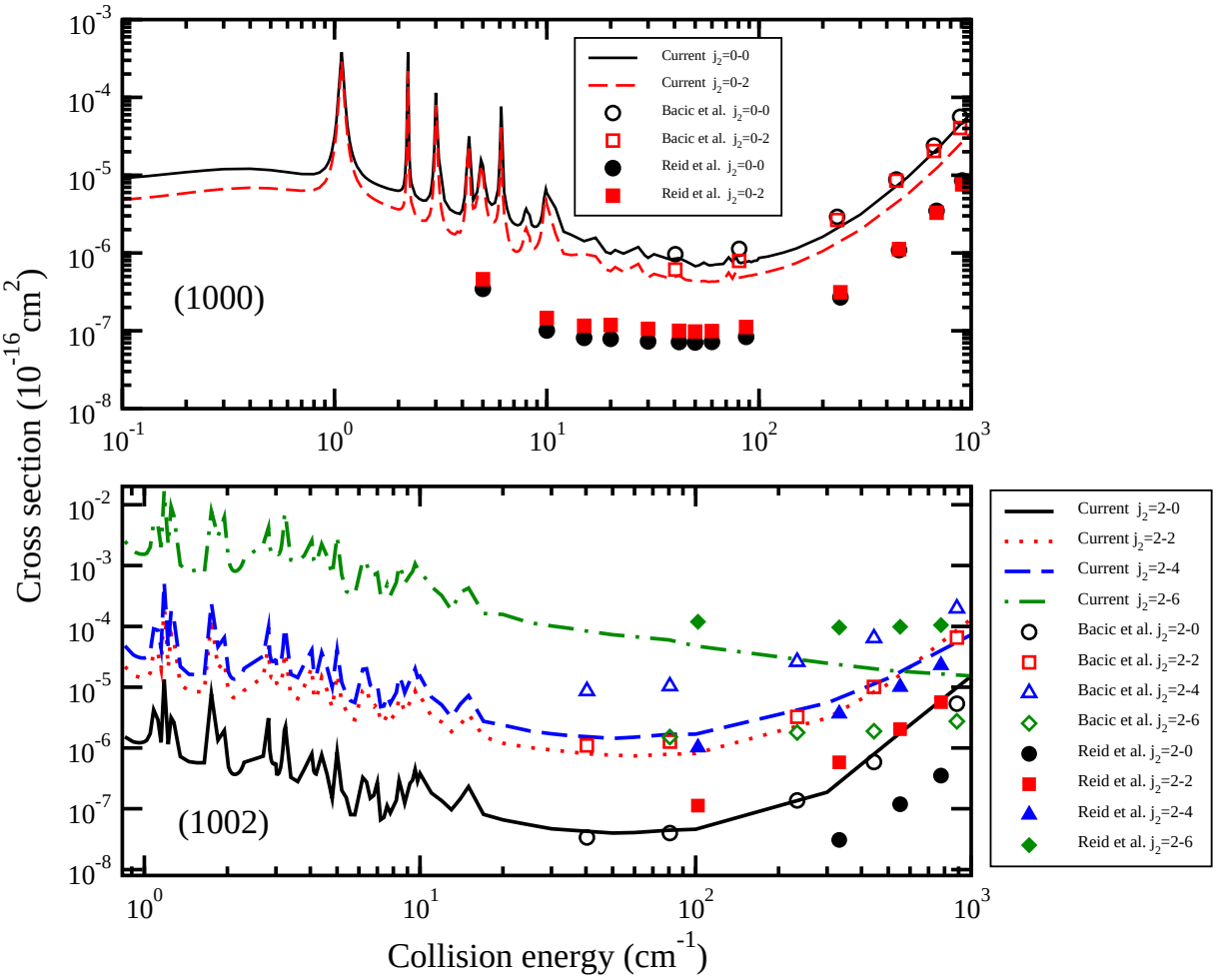

FIG. S10. Total CO–para-H_2 vibrational quenching cross sections for different H_2 states. Total cross sections for the vibrational quenching of CO from initial states (1000) (top panel) and (1002) (bottom panel) to CO($v_1' = 0$) + para-H_2(j_2'=0, 2, 4, 6).

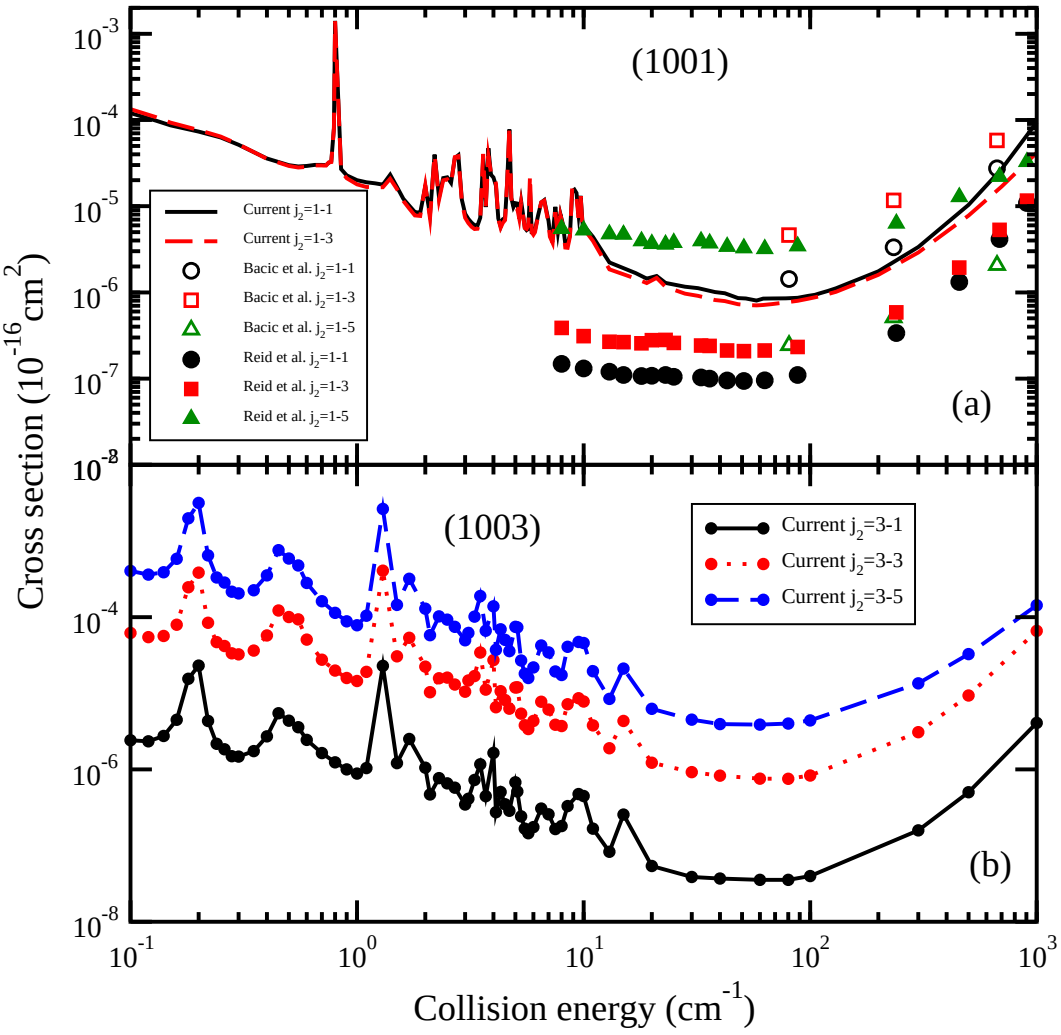

FIG. S11. Total CO–ortho-H_2 vibrational quenching cross sections for different H_2 states. Total cross sections for the vibrational quenching of CO from initial states (1001) (top panel) and (1003) (bottom panel) to CO(v_1'=0) + ortho-H_2(j_2'=1, 3, 5).

SUPPLEMENTARY TABLES

TABLE S1. CO-H_2 rotational excitation errors. RMS error (10^{-16} cm^2) of the three rigid-rotor calculations and V6D in comparison with experiment [S2] at E = 795, 860, and 991 cm^{-1}.

E (cm^{-1})	V6D-full	V6D-EE	V6D-VV	V12
795	0.549	0.546	0.552	0.556
860	0.571	0.598	0.572	0.551
991	0.946	0.989	0.946	0.892

TABLE S2. Parameters used in the CO-H_2 scattering calculations.

	Basis set[a]	N_{θ_1}	N_{θ_2}	N_ϕ	N_{r_1}	N_{r_2}	λ_1	λ_2	No. of channels
4D rotational calculation									
TwoBC	$j_1 = 30$, $j_2 = 2$	14	14	8	1	1	8	4	1344
MOLSCAT	$j_1 = 30$, $j_2 = 2$	14	14	8			8	4	1344
6D TwoBC calculation									
para-H_2-CO	[(0,30;1,20)(0,2)]	14	14	8	20	20	10	6	4258
para-H_2-CO	[(0,22;1,20)(0,4)]	14	14	8	20	20	10	6	7341
para-H_2-CO	[(0,20;1,15)(0,6)]	12	12	8	18	18	8	4	9832
ortho-H_2-CO	[(0,30;1,20)(0,3)]	14	14	8	20	20	10	6	5632
ortho-H_2-CO	[(0,22;1,20)(0,5)]	14	14	8	20	20	10	6	10251

[a] Basis set $[(v_1 = 0, j_{v_1=0};\ v_1 = 1, j_{v_1=1})(v_2 = 0, j_{v_2=0})]$ is presented by the maximum rotational quantum number j_{v_1} and j_{v_2} included in each relevant vibrational level v_1 and v_2 for CO and H_2, respectively.

SUPPLEMENTARY DISCUSSION

Supplementary Note 1: Pure rotational scattering

The V6D PES was adopted in CC scattering calculations using both TwoBC [S3] and MOLSCAT [S4]. Separate calculations were performed with the bond lengths of CO and H_2 fixed at: 1) equilibrium bond lengths, r_1=2.1359 a_0 and r_2=1.4011 a_0, denoted as EE; and 2) vibrationally-averaged bond lengths, r_1=2.13992 a_0 and r_2=1.448736 a_0, denoted as VV. The 4-dimensional (4D) V12 potential of Jankowski *et al.* [S5], which was constructed by averaging over their 6D potential energy data with CO($v_1 = 0$) and H_2($v_2 = 0$) vibrational wave functions, was used in MOLSCAT calculations only. For the rigid-rotor scattering calculations, TwoBC and MOLSCAT give almost identical CO state-to-state excitation cross section using the 4D version of V6D. As an example, Supplementary Fig. S5 displays the CO state-to-state excitation cross sections from $j_1 = 0$ for collision energies of 50, 100, and 500 cm^{-1} due to $H_2(v_2 = 0, j_2 = 0)$ using the V12 potential with MOLSCAT and the two 4D (EE and VV) versions of V6D with TwoBC. Supplementary Fig. S6 gives the differences in these cross sections compared to V6D (full-dimensional) results. There is generally good agreement among all approaches with a small difference depending on which CO and H_2 bond-lengths are adopted. Comparison is also made to the full 6D calculation which agrees best with the rigid-rotor VV results. This confirms both the validity of the rigid-rotor approximation and the suggestion of Jankowski and Szalewicz [S6] that PESs constructed with vibrationally-averaged bond lengths are preferred for scattering calculations. Further, the discrepancy in the rigid-rotor calculations and the 6D results are seen to increase, at least for low j_1', with decreasing collision energy supporting the claim in the main text that accurate prediction of low-energy dynamics requires full-dimensionality.

Antonova *et al.* [S2] measured the relative state-to-state rotationally inelastic cross sections for excitation of CO by H_2 in a crossed molecular beam experiment at collision energies of 795, 860, and 991 cm^{-1} as discussed in the main text. Comparison between the current calculated cross sections and the measurements give a root mean square (RMS) error computed by,

$$\mathrm{RMS} = \sqrt{\frac{\sum_i^N (\sigma_{\mathrm{expt}} - \sigma_{\mathrm{theo}})^2}{N}}, \tag{S1}$$

where σ is the cross section and N the number of data points. The RMS errors for the 4D version of V6D with EE and VV bond lengths, the 4D V12 PES, and the V6D PES are shown in Supplementary Table 1 with the cross sections for the latter two shown in Fig. 2 of the main text. The current V6D results for the final CO j_1' distributions (Fig. 1) are seen to be in excellent agreement with experiment, validating the accuracy of the fitted potential as well as the present scattering calculations.

Chefdeville *et al.* [S7] reported crossed-beam experiments and quantum-mechanical calculations performed for the CO(j_1=0) + H_2(j_2=0) → CO(j_1'=1) + H_2(j_2'=0) process. The 4D V04 PES of Jankowski and Szalewicz [S6] was used in their scattering calculations. To compare with the measurements, the computed cross sections were convolved with the experimental kinetic energy distribution according to,

$$\bar{\sigma}(E) = \frac{1}{\sqrt{2\pi}\delta} \int_0^\infty \sigma(E') \exp\left[-\frac{(E-E')^2}{2\delta^2}\right] dE', \tag{S2}$$

where δ is given by [S7],

$$\delta = \sqrt{2}(0.077 + 0.051E - 3.6 \times 10^{-6}E^2). \tag{S3}$$

The detailed cross sections and discussion are presented in the main text.

Supplementary Note 2: Full-dimensional Scattering calculations

Quenching cross sections

We have performed full-dimensional calculations of the state-to-state cross sections for initial CMSs ($100j_2$), for para-H_2 (j_2=0 and 2), and ortho-H_2 (j_2=1 and 3), for collision energies ranging from 0.1 to 1000 cm^{-1}. As examples, in Supplementary Figs. S7 and S8 the state-to-state quenching cross sections for final states ($0j_1'0j_2$), j_1'=0, 2, 4, $\cdots$, 24 are shown for para- and ortho-H_2, respectively, where $j_2 = j_2'$, i.e., elastic in H_2. The cross sections have similar behaviour and display resonances in the intermediate energy region primarily due to quasibound states supported by the van der Waals well of the interaction potential of the initial channel. Resonances and oscillatory structures, which will be analyzed further in a future publication, appear up to about 100 cm^{-1}, roughly the depth of the van der Waals minimum. Small $|\Delta j_1| = |j_1' - j_1|$ transitions dominate the quenching; the cross sections generally decreasing with increasing j_1' with that for $j_1' = 24$ being the smallest.

The current 6D/CC state-to-state cross sections are summed over j_1' (for $v_1' = 0$) to compare to the total deexcitation 4D cross sections given by Bačić *et al.* [S8, S9], Reid *et al.* [S10], and Flower [S11] as shown for para-H_2 in Fig. 4 of the main text and here for ortho-H_2 in Supplementary Fig. S9. As discussed in the main text there is a two order of magnitude dispersion between the various calculations which may partly be explained by the differing treatments of angular momentum coupling. In the infinite order sudden (IOS) approximation, the internal rotation is neglected (effectively setting $j = 0$), while the coupled-states (CS) approach, which is a centrifugal sudden approximation, allows for the dynamical treatment of rotational transitions. Bačić *et al.* [S8] performed both CS and IOS calculations, but with $j_2 = 0$ (i.e., only para-H_2), while Bačić *et al.* [S9] and Reid *et al.* [S10] used a mixed IOS-CS formalism in which the rotational motion of CO was neglected, but that of H_2 retained, allowing for significant reduction of basis sets. The cross sections from Flower [S11] are likely too large due to an insufficient CO basis, an effect studied by Bačić *et al.* [S8]. In fact, using Flower's basis set in CC calculations on V6D, we obtained significantly larger cross sections than our converged results, verifying the primary cause for the discrepancy. However, in most cases differences are related to the adopted PESs and dimensionality of the scattering approaches.

Quenching rate coefficients

In the calculations of Bačić *et al.* [S8, S9] and Reid *et al.* [S10], the total quenching cross section from state $(v_1 = 1, j_2)$ was obtained by summing the state-to-state quenching cross sections over the final rotational state of H_2, j_2',

$$\sigma(v_1 = 1, j_2 \to v_1' = 0)(E) = \sum_{j_2'} \sigma(v_1 = 1, j_2 \to v_1' = 0, j_2')(E), \tag{S4}$$

allowing for H_2 rotational inelastic transitions (with $v_2 = v_2' = 0$ and no information on j_1 or j_1' as the IOS approximation was adopted for CO in both previous calculations.) By thermally averaging the cross sections over the collision energy, the quenching rate coefficients from $v_1 = 1, j_2$ were obtained.

The total thermal rate coefficients for CO $v_1 = 1 \to v_1' = 0$ vibrational quenching were obtained by summing $k(v_1 = 1, j_2 \to v_1' = 0)(T)$ over all initial H_2 rotational states j_2 weighted by their populations assuming a Boltzmann distribution at T. As observed by

Millikan and Osburg [S12], para-H_2 is a more efficient collision partner than ortho-H_2 for vibrational quenching of CO due to the quasi-resonant transition:
$CO(v_1 = 1) + H_2(v_2 = 0, j_2 = 2) \rightarrow CO(v_1' = 0) + H_2(v_2' = 0, j_2' = 6)$. Guided by the measurements, this quasiresonant process was also theoretically investigated by Bačić *et al.* [S9] and Reid *et al.* [S10] requiring cross sections for rotationally excited H_2 with inelastic H_2 transitions. Supplementary Figs. S10 and S11 compare the j_2 state-to-state cross sections from the earlier work with the current results. As shown in the top panel of Supplementary Fig. S10, the current 6D/CC results are in reasonable agreement with the 4D/CS-IOS calculations of Bačić *et al.* for the $1000 \rightarrow 0j_1'00$ and $1000 \rightarrow 0j_1'02$ cases, but both results are nearly an order of magnitude larger than obtained by Reid *et al.* In the bottom panel of Supplementary Fig. S10, a large scatter in the results is evident for initial state (1002), but generally the cross sections increase with increasing $\Delta j_2 = j_2' - j_2$. The important exception is that contrary to both the current calculations and the 4D/CS-IOS results for Reid *et al.*, Bačić *et al.* find much smaller cross sections for the quasi-resonant process. The V6D/CC results shown in that figure for the quasi-resonant transition were the most computationally time-intensive due to the larger size of the H_2 basis and may represent a lower limit for the cross section at the highest energies.

Supplementary Fig. S11 gives a similar comparison for ortho-H_2 collisions though a quasi-resonant process is not operable due to much larger asymptotic energy differences. Otherwise, the trends are very similar to those noted for para-H_2 collisions, though the current V6D/CC results fall somewhat between the earlier two 4D calculations. Note that we did not consider the H_2 inelastic channel $j_2 = 1 \rightarrow 5$ as Bačić *et al.* [S9] find the cross sections to be more than an order of magnitude smaller than the $j_2 = 1 \rightarrow 3$ transition. This is in contrast to Reid *et al.* who find the $j_2 = 1 \rightarrow 5$ transition to dominate the quenching of (1001). As a consequence, the thermally-averaged rate coefficients for the quenching by ortho-H_2 obtained by Reid *et al.*, shown in Fig. 5a of the main text, are significantly larger than the V6D/CC computation and the experiment. These rate coefficients also include quenching from the initial state (1003), for which the cross sections are shown in the bottom panel of Supplementary Fig. S11, though Reid *et al.* do not tabulate them. Because of the complexity of the system and differences in the PESs and scattering treatments, it is difficult to draw conclusions from one-to-one comparisons of the various calculations. However, the main deficiency in the IOS approach is that it does not resolve the final $CO(j_1')$ channels

which can play a significant role in the cross sections as illustrated in Supplementary Figs. S7 and S8.

SUPPLEMENTARY REFERENCES

[S1] Jankowski, P. & Szalewicz, K. Ab initio potential energy surface and infrared spectra of H_2-CO and D_2-CO van der Waals complexes. *J. Chem. Phys.* **108**, 3554-3565 (1998).

[S2] Antonova, S., Tsakotellis, A. P., Lin, A. & McBane, G. C. State-to-state rotational excitation of CO by H_2 near 1000 cm^{-1} collision energy. *J. Chem. Phys.* **112**, 554-559 (2000).

[S3] Krems, R. V. *TwoBC - quantum scattering program*, (University of British Columbia, Vancouver, Canada, 2006).

[S4] Hutson, J. M. & Green, S. MOLSCAT computer code, Version 14, http://www.giss.nasa.gov/tools/molscat/ (distributed by Collaborative Computational Project No. 6 of the United Kingdom Engineering and Physical Sciences Research Council, Swindon, 1994).

[S5] Jankowski, P., Surin, L. A., Potapov, A., Schlemmer, S., McKellar, A. R. W. & Szalewicz, K. A comprehensive experimental and theoretical study of H_2-CO spectra. *J. Chem. Phys.* **138**, 084307 (2013).

[S6] Jankowski, P. & Szalewicz, K. A new ab initio interaction energy surface and high-resolution spectra of the H_2-CO van der Waals complex. *J. Chem. Phys.* **123**, 104301 (2005).

[S7] Chefdeville, S., Stoecklin, T., Bergeat, A., Hickson, K. M., Naulin, C. & Costes, M. Appearance of low energy resonances in CO-para-H_2 inelastic collisions. *Phys. Rev. Lett.* **109**, 023201 (2012).

[S8] Bačić, Z., Schinke, R. & Diercksen, G. H. F. Vibrational relaxation of CO (n=1) in collisions with H_2. I. Potential energy surface and test of dynamical approximations. *J. Chem. Phys.* **82**, 236-244 (1985).

[S9] Bačić, Z., Schinke, R. & Diercksen, G. H. F. Vibrational relaxation of CO (n=1) in collisions with H_2. II. Influence of H_2 rotation. *J. Chem. Phys.* **82**, 245-253 (1985).

[S10] Reid, J. P., Simpson, C. J. S. M. & Quiney, H. M. The vibrational deactivation of CO(v=1)

by inelastic collisions with H_2 and D_2. *J. Chem. Phys.* **106**, 4931-4944 (1997).

[S11] Flower, D. R. Rate coefficients for the rovibrational excitation of CO by H_2 and He. *Mon. Not. R. Astron. Soc.* **425**, 1350-1356 (2012).

[S12] Millikan, R. C. & Osburg, L. A. Vibrational relaxation of carbon monoxide by ortho- and para-hydrogen. *J. Chem. Phys.* **41**, 2196-2197 (1964).